# Connecting galaxy evolution in clusters with their radial profiles and phase space distribution: results from the IllustrisTNG hydrodynamical simulations

Tara Dacunha,[1]★ Matthew Belyakov [1,2]★ Susmita Adhikari,[3,4] Tae-hyeon Shin [5] Samuel Goldstein[1,6] and Bhuvnesh Jain[1]

[1]*Department of Physics and Astronomy, University of Pennsylvania, 209 S. 33rd St, Philadelphia, PA 19104, USA*
[2]*Division of Geological and Planetary Sciences, California Institute of Technology, Pasadena, CA 91125, USA*
[3]*Department of Astronomy and Astrophysics, University of Chicago, Chicago, IL 60637, USA*
[4]*Kavli Institute for Cosmological Physics, University of Chicago, Chicago, IL 60637, USA*
[5]*Department of Physics and Astronomy, Stony Brook University, Stony Brook, NY 11794, USA*
[6]*Max Planck Institute for Astrophysics, Karl-Schwarzschild-Strasse 1, D-85748 Garching, Germany*

## ABSTRACT

We study the population of galaxies around galaxy clusters in the hydrodynamic simulation suite IllustrisTNG 300-1 to study the signatures of their evolutionary history on observable properties. We measure the radial number density profile, phase space distribution, and splashback radius for galaxies of different masses and colours over the redshift range $z = 0-1$. The three primary physical effects which shape the galaxy distribution within clusters are the galaxy quenching, angular momentum distribution, and dynamical friction. We find three distinct populations of galaxies by applying a Gaussian mixture model to their distribution in colour and mass. They have distinct evolutionary histories and leave distinct signatures on their distribution around cluster haloes. We find that low-mass red galaxies show the most concentrated distribution in clusters and the largest splashback radius, while high-mass red galaxies show a less concentrated distribution and a smaller splashback radius. Blue galaxies, which mostly quench into the low-mass red population, have the shallowest distribution within the clusters, with those on radial orbits quenched rapidly before reaching pericentre. Comparison with the distribution of galaxies from the Dark Energy Survey survey around Sunyaev–Zeldovich clusters from the Atacama Cosmology Telescope and South Pole Telescope surveys shows evidence for differences in galaxy evolution between simulations and data.

**Key words:** galaxies: clusters: general – galaxies: evolution – galaxies: kinematics and dynamics – galaxies: star formation.

## 1 INTRODUCTION

Galaxies evolve within the potential wells of massive dark matter haloes, some of the largest of these bound structures are known as galaxy clusters. These are relatively easy to observe and characterize and provide an excellent laboratory to test the predictions of hierarchical structure formation and galaxy evolution.

It has been known that galaxies that live in these dense environments are often elliptical galaxies that appear to have little or no active star formation (Oemler 1974; Dressler 1980; Dressler & Gunn 1983; Balogh et al. 1997; Poggianti et al. 1999). Various physical processes have been invoked to explain this galaxy star formation/morphology–density relationship. This phenomenon is primarily expected to arise from astrophysical processes within the galaxy cluster that remove the reservoirs of cold gas from infalling galaxies and prevent them from forming stars. Various processes, with graphic names, like strangulation (Larson, Tinsley & Caldwell 1980), ram-pressure stripping (Gunn & Gott 1972), and harassment (Abadi, Moore & Bower 1999) of galaxies falling into the hot intracluster environment

cause the star formation rates of galaxies to decrease over time as they orbit through a halo's potential well.

Recently, measurements of the splashback radius ($R_{sp}$) have provided new insight into understanding the evolution of collapsed structures like dark matter haloes in the Universe (More et al. 2016; Baxter et al. 2017; Chang et al. 2018; Shin et al. 2019, 2021; Zürcher & More 2019; Murata et al. 2020; Adhikari et al. 2021). The splashback feature appears at the edge of dark matter haloes, separating the inner virialized, or multistreaming regions, from the infall regions, forming the boundary of dark matter haloes (Adhikari, Dalal & Chamberlain 2014; Diemer & Kravtsov 2014; More, Diemer & Kravtsov 2015; Shi 2016). The splashback surface forms near the first apocentre of the most recently infalling material. In idealized models of halo collapse there is a density caustic at splashback (Fillmore & Goldreich 1984; Lithwick & Dalal 2011; Adhikari et al. 2014), but in stacked clusters it manifests itself as a steepening of the slope of the density profile in a narrow localized region, where the inner halo term sharply falls off, giving away to a shallower infall density. Since the radial velocity of dark matter particles or satellite galaxies is low near the turnaround radius, they cluster at $R_{sp}$ (Adhikari et al. 2014). For an observed galaxy cluster, $R_{sp}$ is often defined as the radius where the logarithmic slope of the

★ E-mail: tdacunha@sas.upenn.edu (TD); mattbel@sas.upenn.edu (MB)

galaxy number density profile or the dark matter density reaches a minimum (maximum steepness).

As the splashback radius traces the first apocentre, it can also directly be associated with a time-scale, i.e. the time taken for a galaxy or a dark matter particle to make one passage through a pericentre and reach its orbital apocentre from first infall (Adhikari et al. 2021). Therefore, if a population of galaxies shows a splashback-like feature, we can associate an average time-scale to it. As intracluster processes that influence the evolution of galaxies are naturally sensitive to the time spent by a galaxy within the cluster potential it is important to understand how galaxy properties and their distribution in observed clusters can inform us about different cluster processes.

In this paper, we investigate the connection between galaxy evolution and the colours of observed galaxies and study how different evolutionary histories leave their imprint on the phase space distributions and the shape of the full radial profile of a population of galaxies. We use the state-of-the-art IllustrisTNG (Nelson et al. 2018) suite of hydrodynamic simulations for this analysis. Donnari et al. (2021) analysed quenching mechanisms in IllustrisTNG 100-1 and 300-1. They find that galaxies in IllustrisTNG show primarily two quenching pathways, determining that low-mass galaxies experience strong amounts of environmental quenching, while high-mass galaxies go through mass quenching driven by active galactic nuclei (AGNs) and mergers. We study how these pathways leave signatures in the cluster field. O'Neil et al. (2021) have characterized the splashback radius of galaxies and dark matter in clusters in IllustrisTNG as a function of halo properties. In this work, we study in detail how the distribution of galaxies depends on the galaxy star formation properties and explore how we can use these distributions to constrain models of galaxy quenching in observations. We complement and expand upon the results from Shin et al. (2019) and Adhikari et al. (2021), who have examined the galaxy colour and splashback connection by forward modelling observations from cold dark matter (CDM) *N*-body simulations.

In particular, the assembly history of galaxies in a cluster mass halo is imprinted on their spatial and velocity distribution within the cluster. The overall radial number density of galaxies is sensitive to various processes like tidal disruption, dynamical friction, and quenching, each of which are sensitive to the angular momentum and infall time of galaxies into the cluster. Moreover, the relative importance of the different processes can change as a function of halo properties such as accretion rate, redshift, and cluster age. Most observational studies of the splashback radius compare with results from CDM–*N*-body simulations, assigning galaxies to subhaloes, in this paper, we attempt to marginalize over the uncertainty in the subhalo–galaxy connection and compare directly to hydrodynamic simulations. While the details of the feedback model in hydrodynamic simulations may still be uncertain, it is ideal for studying the overall expected trends with galaxy properties. Comparison with data can then be helpful for both constraining the models in theory space and also for data interpretation. In this paper, we primarily focus on galaxy populations separated by their colour and magnitude properties, to understand how these different populations inhabit clusters.

This paper is organized as follows. In Section 2, we briefly describe the IllustrisTNG simulation and the halo and galaxy selection method we use. In Section 3, we describe our colour-mass population split and how we determine its location, discuss the differences in evolutionary history of colour and mass, as well as the star formation rate of the populations. In Section 4, we compare the phase space distributions of the populations, emphasizing the distribution of gas,

dark matter, and total mass in phase space. In Section 5, we first compare the galaxy number density profiles and resulting splashback feature for each of the three different colour-mass populations over redshift. We then make comparisons to splashback results in data from (Shin et al. 2019) and (Adhikari et al. 2021). We also examine the potential for dynamical friction as an explanation for the differences in the splashback feature between populations. In Section 6, we summarize our results, compare to other work, propose observables, and discuss further directions.

## 2 SIMULATION

We conduct our analysis on the IllustrisTNG 300-1 data set as presented in Nelson et al. (2018), Springel et al. (2018), Marinacci et al. (2018), Pillepich et al. (2018), and Naiman et al. (2018). IllustrisTNG is a suite of large volume cosmological magnetohydrodynamic simulations which are based on an improved version of the original Illustris galaxy formation model and rely on the moving-mesh code AREPO (Springel 2010; Nelson et al. 2018; Weinberger, Springel & Pakmor 2020). All IllustrisTNG simulation runs use cosmological parameters from the Planck Collaboration: $\Omega_m = \Omega_{dm} + \Omega_b = 0.3089$, $\Omega_b = 0.0486$, $\Omega_\Lambda = 0.6911$, $\sigma_8 = 0.8159$, $n_s = 0.9667$, with a Hubble constant of $H_0 = 100\,h\,\mathrm{km\,s^{-1}\,Mpc^{-1}}$, where $h = 0.6774$ (Planck Collaboration VI 2018).

We use the TNG300-1 high-resolution simulation. The TNG300 simulation is run within a periodic cube with a side length of 302 Mpc, with TNG300-1 being the highest resolution box. TNG300-1 has an initial $2 \times 2500^3$ cells/particles, with a gas cell mass of $1.1 \times 10^7\,h^{-1}\,\mathrm{M_\odot}$, dark matter cell mass of $4.0 \times 10^7\,h^{-1}\,\mathrm{M_\odot}$, and baryonic matter cell mass of $7.6 \times 10^6\,h^{-1}\,\mathrm{M_\odot}$. Dark matter particles in the simulation have a gravitation softening length of 1.5 kpc in physical units for $z \leq 1$ and comoving units for $z > 1$ (Nelson et al. 2021). The public release provides 99 snapshots between $z = 20$ and $z = 0$. The large volume and high resolution make it ideal to study a large dynamic range of halo masses from cluster mass objects to their satellite galaxies.

### 2.1 Cluster and galaxy selection

We select 10 snapshots from TNG300-1 between $z = 0$ and $z = 1$. Gravitationally bound structures are located by the simulation using the SUBFIND algorithm (Springel et al. 2001; Dolag et al. 2009). These structures are subsequently linked with each other and nearby particles using a friends-of-friends (FoF) algorithm (Davis et al. 1985).

Our cluster sample consists of haloes with $M_{200m} > 5 \times 10^{13}\,h^{-1}\,\mathrm{M_\odot}$. Note that this is smaller than the mass threshold of clusters typically used in the splashback analysis of observational data; however, we use this threshold to give us good statistics in the IllustrisTNG-300 box which has a significantly smaller volume than galaxy surveys like the Dark Energy Survey (DES; The Dark Energy Survey Collaboration 2005) and The Hyper Suprime Cam survey (Aihara et al. 2018), and therefore fewer massive clusters above the mass threshold used in data. We examine these populations in IllustrisTNG over different redshifts, but we primarily focus on the TNG300-1 snapshot 66 at redshift, $z = 0.52$. Our cluster sample consists of 311 haloes with a mean halo mass of $M_{200m} = 10^{13.9}\,h^{-1}\,\mathrm{M_\odot}$. We make this choice of redshift to compare with observational results from Shin et al. (2019) and Adhikari et al. (2021) (see Section 5.3), where the mean redshift of the sample is $z = 0.49$. When comparing with data radial distributions, we will present our results in units of $r/R_{200m}$.

**Table 1.** The number of haloes with mass greater than $5 \times 10^{13}\, h^{-1}\, M_\odot$ and galaxies of each colour-mass population that are within $7\, R_{200m}$ of a massive halo. The galaxy numbers include double-counted galaxies, since a galaxy can be within $7\, R_{200m}$ of multiple massive haloes. The proportion of both high-mass and low-mass Red galaxies to total number of galaxies, increases at later times which is in line with the notion of quenching.

| Redshift | 0 | 0.1 | 0.2 | 0.3 | 0.4 | 0.5 | 0.6 | 0.7 | 0.8 | 1.0 |
|---|---|---|---|---|---|---|---|---|---|---|
| Haloes | 684 | 599 | 530 | 454 | 390 | 311 | 279 | 214 | 169 | 118 |
| Blue galaxies | 116 692 | 116 429 | 113 127 | 107 374 | 99 527 | 86 337 | 80 581 | 67 246 | 56 463 | 42 705 |
| Red$_{high}$ galaxies | 36 400 | 29 962 | 24 482 | 19 866 | 15 649 | 10 932 | 9215 | 6648 | 4778 | 2841 |
| Red$_{low}$ galaxies | 199 446 | 160 292 | 128 988 | 102 991 | 80 174 | 56 055 | 46 447 | 33 062 | 23 465 | 13 026 |

For the purposes of this paper, we define a galaxy to be an IllustrisTNG-defined subhalo[1] with stellar mass greater than $10^8\, h^{-1}\, M_\odot$. These are found using the SUBFIND algorithm (Springel et al. 2001; Dolag et al. 2009), each 'subhalo', is a gravitationally bound structure that is defined using an FoF algorithm. The most bound particle is defined as the centre of the halo. As we intend to study the total distribution of galaxies within the cluster and in its neighbourhood and make comparisons with data, we use all galaxies that are within $7\, R_{200m}$ of the cluster halo centre.

The total numbers of haloes and galaxies for each redshift snapshot are summarized in the Table 1.

## 3 PROPERTIES OF GALAXIES IN ILLUSTRIS

In this section, we study the properties of galaxies in the IllustrisTNG simulations, focusing on their total and stellar masses, colour, and star formation rates. Notably, we find that galaxies around clusters in IllustrisTNG can be divided into three distinct groups in colour-mass space. We examine the evolutionary history of these three groups in colour-mass space along with their star formation rates in order to probe the differences between them. We compare our colour-mass splits to the colour splits made in DES/ACT data (Adhikari et al. 2021) and others in IllustrisTNG (Nelson et al. 2018).

### 3.1 Colour-mass populations

We use the photometric data in IllustrisTNG for each galaxy to analyse the colour distribution of galaxies in our sample. Photometric data in the *griz* bands in Illustris are based on the SDSS Camera X Response Function (airmass = 1.3). The magnitudes given in *griz* are all rest frame, and are absolute (AB system). We use $g - r$ for colour throughout this paper.

In Fig. 1, we show the distribution of galaxies in the simulation at $z = 0.52$ in colour-mass space. The total mass of a galaxy in IllustrisTNG includes the stellar mass, dark matter mass, gas mass, and black hole mass associated with that given galaxy. We choose the total mass to define our populations as we focus on the dynamics of galaxies in the gravitational field of the cluster, which is determined primarily by their total mass, rather than their stellar mass. We note that there are three distinct populations in this space. While the usual red and blue sequence of galaxies is visible, we note that the galaxies in the red sequence can, in fact, further be divided into two distinct populations; we therefore define a different categorization of galaxies for this work: a Blue population with low $g - r$ colours, and two Red populations with low and high total masses. Note that the low- and high-mass Red galaxies are also, on average, lower and higher in $g - r$ colour, respectively. In order to isolate these populations,
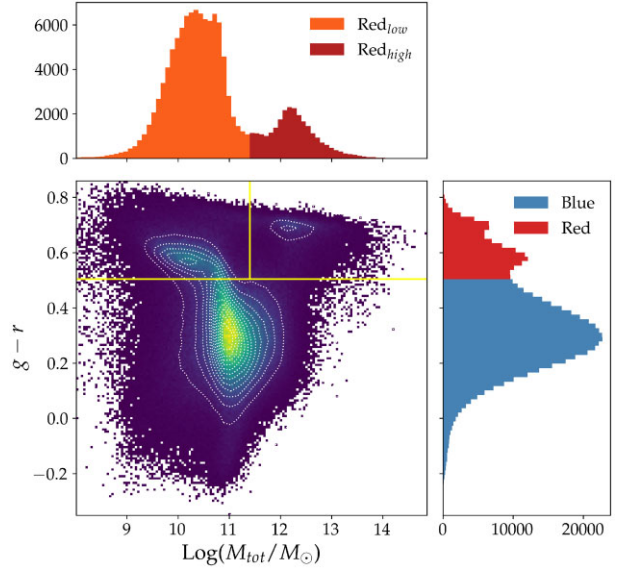
[1] In SUBFIND, a halo is generally called a subhalo, it does not necessarily mean it is within the virial radius of a larger structure.

**Figure 1.** Colour-mass plot of our galaxy sample at $z = 0.52$ in IllustrisTNG. Three distinct colour-mass populations are visible. The one below $g - r$ of approximately 0.5 is 'Blue', the one above $g - r = 0.5$ and with total mass less than $10^{11.4}\, h^{-1}\, M_\odot$ is 'Red$_{low}$', with the last group being 'Red$_{high}$'. The top and right histograms display the one-dimensional distributions of the galaxies in colour and total mass space. The top histogram of total mass includes only the galaxies defined as Red to illustrate the mass cuts between the two Red populations. The colour splits used at this redshift are indicated as yellow lines in the main plot.

we use a series of Gaussian mixture models and test the Bayesian information criterion (BIC) to obtain the most preferred models for splitting the colour-mass space. The BIC for a Gaussian model with independent model errors is given by

$$\mathrm{BIC} = n\ln(\widehat{\sigma_e^2}) + k\ln(n), \qquad (1)$$

where $n$ is the number of observations, or in this case the number of galaxies, $\widehat{\sigma_e^2}$ is the error variance, and $k$ is the number of parameters estimated, which increases with the number of Gaussian curves used to fit the data. A larger BIC value for the same data implies the model is less preferable. We first define a Red and Blue population using the distribution shown in the histogram on the right-hand panel of Fig. 1. We find that a single Gaussian has a significantly higher BIC than using two Gaussians ($\Delta$BIC $\gg$ 10). Although three Gaussians fit to $g - r$ data have a lower BIC than the two Gaussian fit, the resulting two Red populations from the three Gaussian fit are both bimodal in mass, thus there is no reason to prefer this split. We then define the exact boundary between the two resulting colour-only populations by the intersection of the two Gaussian curves from the mixture model; at $z = 0.52$, we split the populations at $g - r = 0.505$. We then again use a Gaussian mixture model to determine the

mass split between the two red populations in total mass, which we term Red$_{high}$ and Red$_{low}$. The BIC for the split using two Gaussians is again significantly lower than the single Gaussian, suggesting that splitting the two populations is preferred over treating them as a single 'red' population. At $z = 0.52$, the mass split divides Red$_{high}$ and Red$_{low}$ at a mass of $10^{11.4} \, h^{-1} \, M_{\odot}$. We repeat the same method of Gaussian mixture models to determine individual splits for each IllustrisTNG snapshot considered in our analysis.

We note that our colour selection is apparently a deviation from earlier studies of colour evolution in IllustrisTNG like Nelson et al. (2018), which studies the star formation properties of central galaxies, and Donnari et al. (2021), where the focus was mainly on quenched fractions using star formation rate, and therefore was mainly studying a binary distribution of properties. As we will eventually study a population of galaxies, primarily around clusters, that are strongly biased objects, we isolate the clear overdensity of massive red galaxies living typically living in group mass haloes. We therefore study the evolution of these three populations separately.

Note that the photometric information used in this paper is not dust-corrected. However, we find that the three populations separate out distinctly in the colour-total mass space even when the dust-correction is applied, the only difference being that the red and blue separation is at a marginally redder colour.

### 3.2 The star-forming main sequence

We examine how the three galaxy populations defined in the colour-$M_{tot}$ space lie w.r.t. to the star-forming main sequence (SFMS; Popesso et al. 2018). Galaxies tend to lie on this roughly linear main sequence, where the overall trend is that galaxies with larger stellar mass have higher log star formation rates (Donnari et al. 2019). In Fig. 2, we plot the logarithmically scaled star formation rate and stellar mass, along with mean values in mass bins to represent the SFMS.[2] The colours in the lower plot of the figure indicate $g - r$ colour, with the lighter and darker red points largely coinciding with the Red$_{low}$ and Red$_{high}$ populations, respectively.

We find that both Blue and Red$_{low}$ galaxies tend to follow the SFMS and are consistent with the findings of Donnari et al. (2019). The mean star formation rate for Red$_{low}$ galaxies is lower than Blue ones. For both galaxy samples, we recover a linear relationship between log SFR and log stellar mass for the mass range of $10^9$ to $10^{10.5} \, h^{-1} \, M_{\odot}$. However, the high-mass and higher $g - r$ Red$_{high}$ galaxies, do not lie on the main sequence. As less red galaxies increase in log SFR along with mass, at high mass, we encounter galaxies with extremely low SFR that are significantly redder. This reflects what has been termed as a 'flattening' or 'bending' of the SFMS at stellar masses greater than $10^{10.5} \, M_{\odot}$, which is most similar to our Red$_{high}$ sample (Popesso et al. 2018).

In the following subsection, we examine evolutionary processes associated with these galaxies.

### 3.3 Galaxy population histories in colour-mass space

We use the LHaloTree merger tree for the IllustrisTNG 300-1 simulation to examine the histories of the three colour-mass populations defined in the previous section over a redshift range of $z = 14$ to $z = 0$. At $z = 0.52$, we randomly sample 1000 each of Blue, Red$_{high}$,
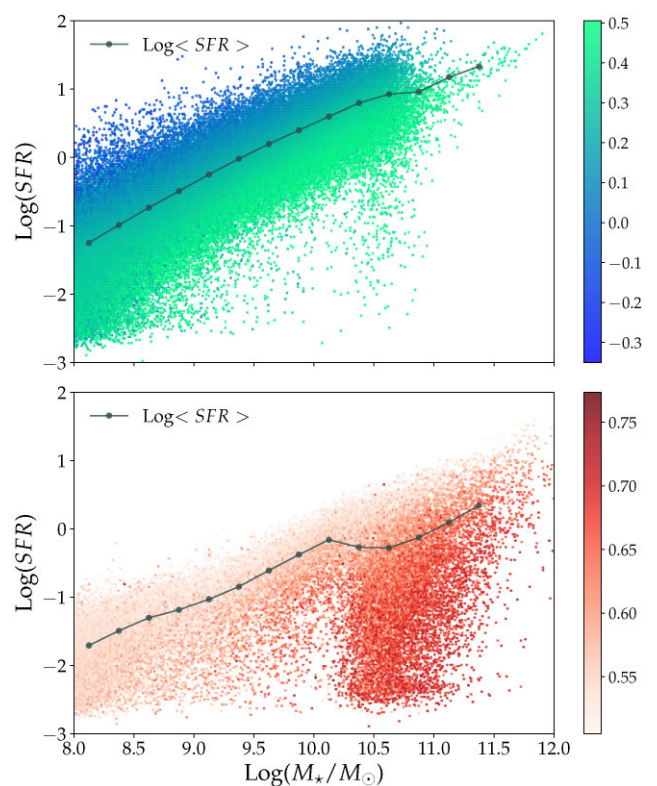
<sup>2</sup>This plot does not include the galaxies to which IllustrisTNG assigns a value of SFR = 0 due to resolution effects, which corresponds to 2.5 per cent of Blue, 43 per cent of Red$_{high}$, and 75 per cent of Red$_{low}$ galaxies at $z = 0.52$.
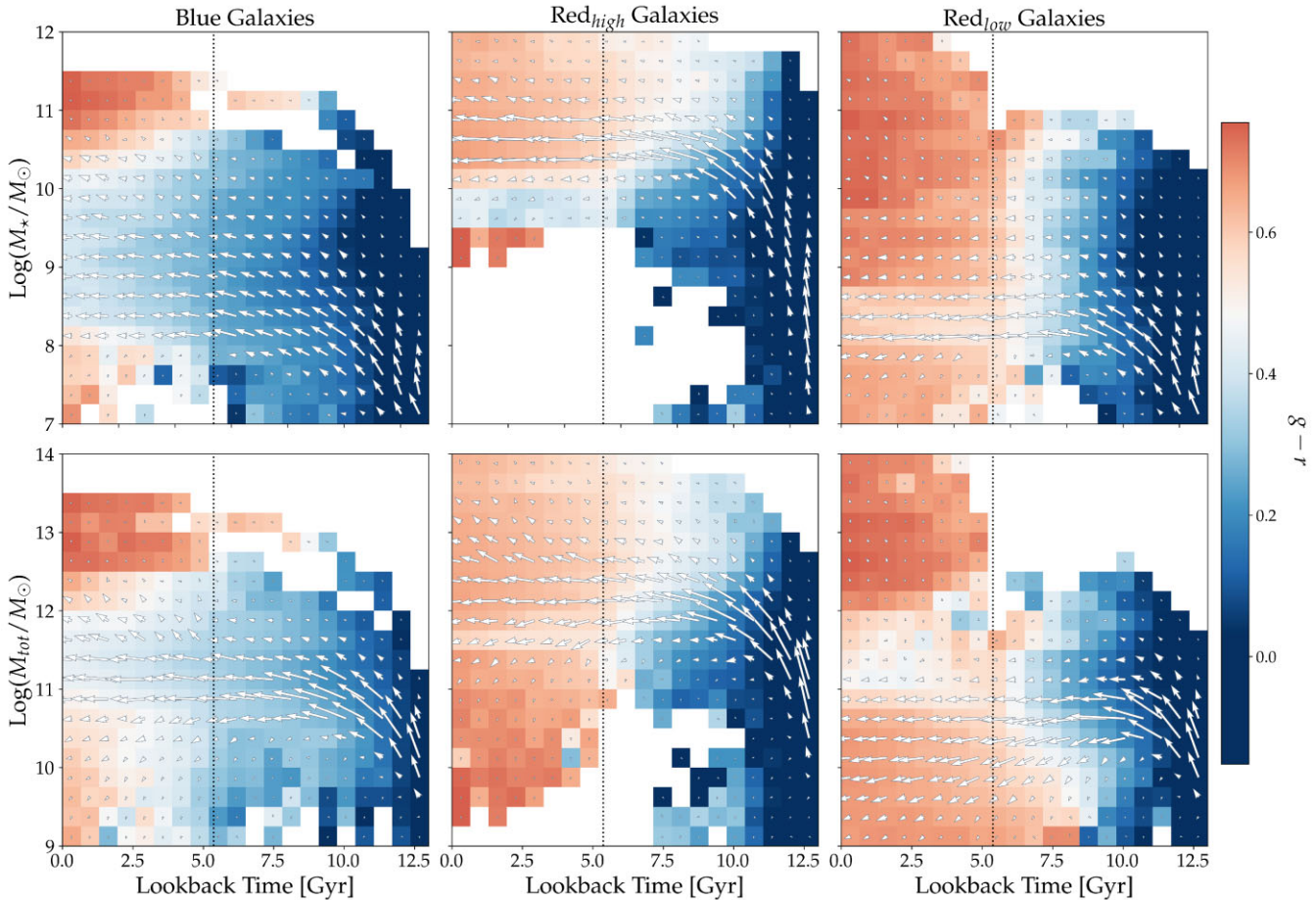


**Figure 2.** SFR main sequence for $z = 0.52$. These two plots show log SFR versus log stellar mass for all galaxies colour-coded by their $g - r$ colour, overplotted by a black line showing the log mean SFR in stellar mass bins. The upper plot displays the Blue sample, with the bluer and greener points indicating the higher and lower $g - r$ galaxies in the Blue population. Colour is correlated with higher SFR at all stellar mass ranges for the Blue population, following the SFR main sequence. The lower plot includes the entire Red sample, i.e. both Red$_{low}$ and Red$_{high}$ galaxies, with redder points indicating redder galaxies. The reddest galaxies display a characteristic and exaggerated flattening of the main sequence.

and Red$_{low}$ galaxies from IllustrisTNG, tracing their histories in mass and colour both forwards and backwards in time. We use the main progenitor branch and descendent branch to trace mergers and histories. The main progenitor of a subhalo is defined as the parent subhalo which has the largest combined mass in its history. In Fig. 3, we plot the pathways which each of our three populations take in mass-time space, showing the average colour of galaxies at that time and mass. We highlight some of the most notable features below.

First, as expected, we find that all galaxy populations begin as blue galaxies with low stellar masses at early times. With time, galaxies evolve into redder colours, but the colour evolution for the three populations is distinct from each other. In general, galaxies become red either when they reach a certain mass, or by environmental effects that is also accompanied by a loss in the total mass of the halo presumably due to tidal effects. We also note that the mass assembly itself is different, in particular galaxies that are in the Red$_{high}$ population tend to assemble their mass earlier in time than lower mass Blue and Red$_{low}$ galaxies.

The Red$_{high}$ population at $z = 0.52$ originates as Blue galaxies, which first increase in total and stellar mass without significantly reddening, and then upon reaching a critical mass, quickly quench into the massive Red$_{high}$ population. This is indicative of an AGN-driven feedback that is triggered at a critical mass threshold (Nelson et al. 2018; Weinberger et al. 2018; Terrazas et al. 2020; Donnari

**Figure 3.** Evolution of a sample of 3000 galaxies sampled equally from the three galaxy populations: Blue (left), Red$_{high}$ (middle), and Red$_{low}$ (right). The pixel colour in each panel shows the average $g - r$ colour of all the galaxies in that pixel. The length and direction of the arrows represent the average change in mass and time between consecutive simulation snapshots. The arrow thickness represents the number of galaxies within each bin. The vertical black dotted line in each panel indicates the lookback time at $z = 0.52$, the redshift at which the populations are identified in this figure.

et al. 2021) and progresses relatively quickly. At later times, some of these Red$_{high}$ galaxies lose total mass while maintaining their stellar mass, presumably from tidal mass-loss by merging into cluster-sized objects. Red$_{low}$ galaxies, on the other hand, begin to quench at a lower stellar and total mass, and quickly enter a phase where they begin to lose total mass, implying that their haloes are getting stripped as they undergo infall into a larger object. We note that the mass-loss begins after the galaxies are significantly reddened. We also note that while a part of the Red$_{low}$ galaxies at $z = 0.52$ appears to become a population of high $g - r$ and high-mass galaxies at late times (presumably through mergers and the like, the arrow size in those bins indicates that it is a relatively small fraction of the population compared to those that maintain or lose mass as the redden further.

We calculate the average time it takes the galaxies in our Red$_{low}$ and Red$_{high}$ samples selected at $z = 0.52$ to travel from a $g - r$ value of 0.0–0.5. Galaxies that end up as Red$_{low}$ take on average $4.79 \pm 1.33$ Gyr to traverse that colour range. Galaxies that end up as Red$_{high}$ tend to quench faster with an average time-scale of $4.08 \pm 1.66$ Gyr. These distinct Red populations are the products of different mechanisms with different rates. The large spread of Red$_{high}$ quenching times could also indicate that the population is formed through multiple quenching mechanisms with at least one acting rapidly compared to the quenching of Red$_{low}$ galaxies.

We note that, at late times, Blue galaxies at $z = 0.52$ that end up quenched by $z = 0$ do not appear to lose total mass, which is likely a result of them mostly being in fields and voids (low-density regions).

Overall, we find evidence for two dominant quenching scenarios, consistent with those proposed in literature. Mass-triggered quenching and environmental quenching are visible and distinguishable in these two distinct Red galaxy populations in IllustrisTNG. At our given fiducial redshift, the low-mass Red galaxies (Red$_{low}$) are typically environmentally quenched, reflecting the effects of environmental processes such as tidal stripping, ram pressure stripping, starvation, and harassment (Gunn & Gott 1972; Abadi et al. 1999; Contini et al. 2020; Donnari et al. 2021). On the other hand, the massive red galaxies (Red$_{high}$) are quenched by both internal processes, such as AGN feedback, and mergers.

## 4 PHASE SPACE DISTRIBUTION OF GALAXY PROPERTIES

In this section, we study the distribution of galaxies and galaxy properties in the phase space of dark matter haloes. The phase space of haloes is the two-dimensional space of the radial velocity and the radial distance from the halo centre. This space provides an intuitive way to look at the evolution of a dark matter halo as different regions of this space can be mapped on to different times
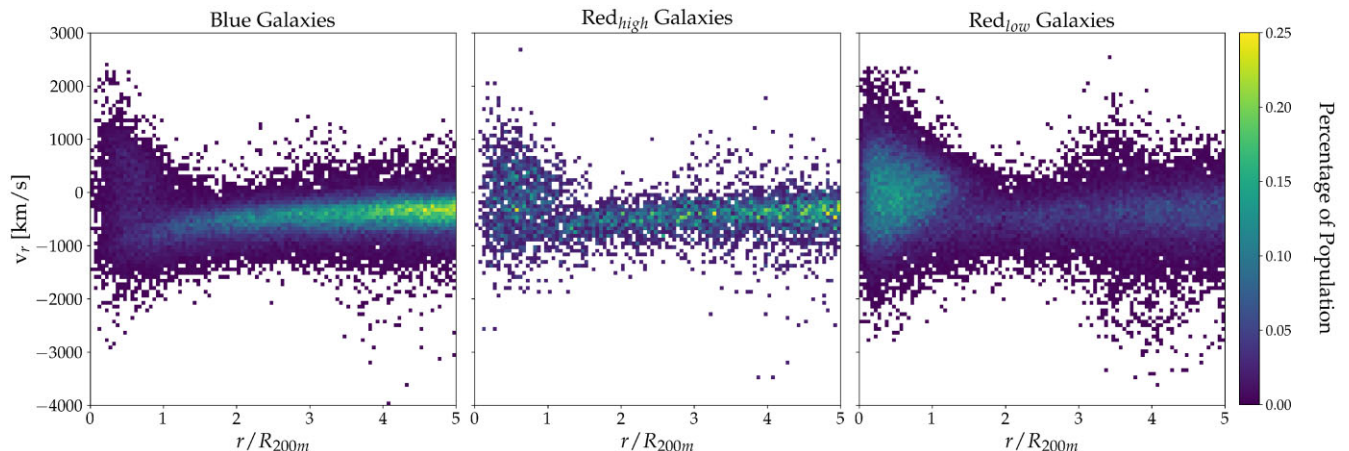
**Figure 4.** Stacked 3d phase space diagrams for the three colour populations (Blue, Red$_{low}$, and Red$_{high}$ going from left to right) at $z = 0.52$. The colour indicates the percentage of the population in that 2d bin, i.e. yellower bins indicates the presence of more galaxies. All three populations show clearly defined infall streams and multistreaming regions. Blue galaxies are predominantly located in the infall stream, with their density falling off towards the multistreaming region. Red$_{high}$ galaxies (middle panel) are split evenly between infall and multistreaming regions, with the lowest radial velocity dispersion in the infall stream. Red$_{low}$ galaxies are present across the entire virialized region as well as the infall stream, and have the highest radial velocity dispersion in the infall stream.

in the halo's formation history. In the idealized CDM spherical evolution (Fillmore & Goldreich 1984), every particle follows a unique trajectory in this space as the dark matter sheet warps with time. Galaxies that are collisionless tracers of the dark matter potential are also expected to follow similar phase space trajectories.

Phase space diagrams of the radial velocities of particles prominently display two distinct regions in and around clusters: the infall stream and the multistreaming region. Defined as the steepening of the density profile at the location of first turnaround, the splashback radius traces the boundary between these two regions visible in phase space. Matter on its first infall resides in the infall stream, extending across the range of radii in the diagram. Matter already 'virialized' and orbiting in the cluster resides in the multistreaming region, extending to approximately the splashback radius with a range of radial velocities.

Moreover, the spherically averaged radial density profile of a halo is the integral of the phase space distribution in the velocity direction. Therefore, galaxies occupying different regions in phase space imprint their signatures on the observed shape of the density profile. While this property was exploited in Adhikari et al. (2021) to infer the times of infall of different galaxy populations and also to constrain a simple quenching model, we directly test this hypothesis in this work using hydrodynamic simulations to explore whether observable properties of galaxies indeed separate out in phase space and what their distributions help us infer about galaxy evolution.

### 4.1 Distribution of galaxy colour

In this section, we study the distribution of galaxy colour in the phase space of dark matter haloes. We divide our galaxies into three populations namely Blue, Red$_{high}$ and Red$_{low}$, as described above, and analyse their distribution in phase space. In Fig. 4, we plot the stacked phase space for the three colour-mass populations at $z = 0.52$. We divide the two-dimensional space of $v_r$ and $r/R_{200m}$ into 100 bins along the radial direction and 100 bins along the velocity direction. The colour of the bins indicates the number density of galaxies in each bin. We note that the three different populations display distinct behaviour in phase space. We highlight the most significant features of these distributions: Blue galaxies are dominant in the infall stream

of the cluster whereas the low-mass Red galaxies (Red$_{low}$) occupy the full extent of the virialized region along with the infall stream. The high-mass Red galaxies (Red$_{high}$) appear to be concentrated near the centre of the cluster and appear to have a lower radial velocity envelope compared to both the Blue and Red$_{low}$ population. We also note that in the infall regions ($r/R_{200m} > 1.5$ Mpc $h^{-1}$), i.e. beyond the splashback radius, both Blue and Red$_{low}$ galaxies tend to have a broad radial velocity dispersion compared to the Red$_{high}$ galaxies.

The phase space distribution of these different populations can be well understood by their evolutionary pathways. First, if Blue galaxies are preferentially quenched inside the cluster, they would be most dominant in the infall stream. Also, if Blue galaxies get quenched into Red ones, the multistreaming region in the phase space would be dominated by Red galaxies with time, which is clearly seen in the rightmost panel of Fig. 4. However, we note that the most massive Red galaxies presumably fall into the cluster as central galaxies of groups that are red even before infall into the cluster. These massive objects tend to sink to the centre because they lose momentum due to dynamical friction and self-friction (see Section 5.3), and appear to be confined within a low radial velocity envelope, that only extends out to about $\sim 0.5 R_{sp}$.

Analysing the infall streams, i.e. with $r > R_{sp}$, we note that the Red$_{low}$ and Blue galaxies tend to extend out as clouds from the narrow infall stream. This is due to the fact that a significant fraction of these galaxies fall in as satellites of higher mass groups, with their own phase space structures. We note that Red$_{low}$ galaxies tend to live in these high-velocity clouds. This further distinguishes them from Red$_{high}$ galaxies which tend to live in the narrow infall stream, likely as field galaxies or as centrals of the aforementioned infalling groups. In Appendix C, we also plot the line-of-sight (LOS) velocity dispersions of the three populations in three cluster-centric radial bins. The LOS velocities are often used in spectroscopic surveys to infer quenching time-scales (Oman & Hudson 2016; Adhikari et al. 2019) and to infer halo masses (Anbajagane et al. 2022), we note that the dispersions can change significantly as a function of radius and galaxy colour.

In Fig. 5, we plot the stacked phase space of the clusters with bin colour weighted by the mean $g - r$ colour of all the galaxies in that bin. We plot this colour-weighted phase space at three
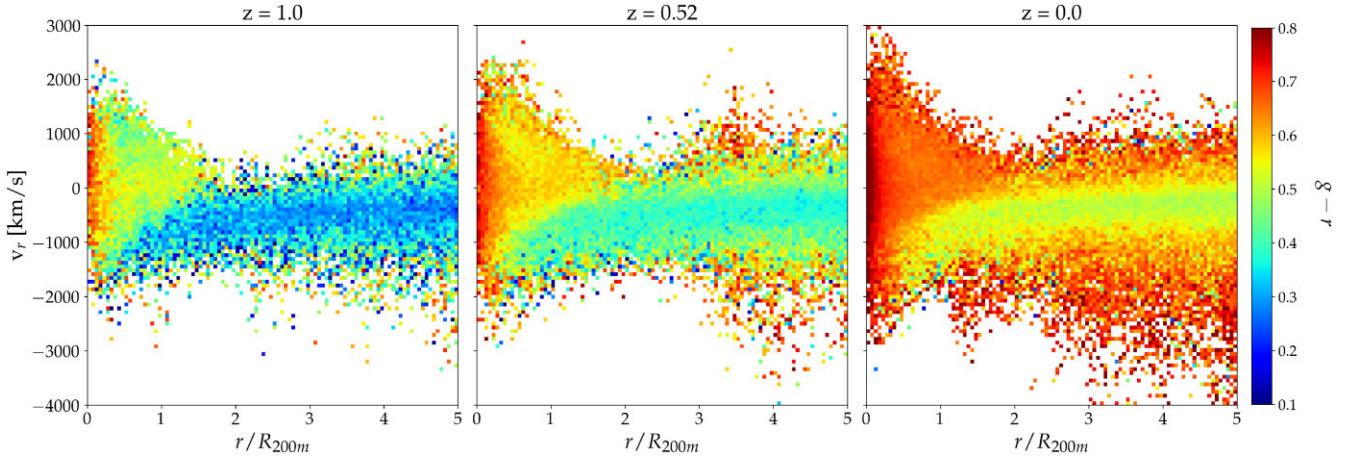
**Figure 5.** Stacked 3d phase space diagrams for all galaxies in our sample at three redshifts as indicated above each panel. The points are coloured by the mean $g - r$ colour in a given bin of the 2d histogram. At earlier times, the infall stream is predominantly composed of blue galaxies, with only a few redder galaxies at high velocities. At later times, as more structure grows, the infall stream widens significantly, with higher (absolute value) velocities dominated by redder galaxies. The red galaxies at high radial velocities are undergoing infall as parts of groups.

different redshifts, $z = 0, 0.52, 1.0$. We note that at all redshifts, the infall stream remains dominated by bluer galaxies. Generally, the galaxy population around a cluster gets redder with time. We note particularly that the velocity dispersion of the infall stream gets larger at late times as structure grows, and the higher velocity tails are occupied by red galaxies quenched pre-infall.

In the following section, we examine the different components of these galaxies in the phase space, i.e. we study the relative ratios of gas, stellar mass and dark matter as a function of their radial velocity and distance from the cluster centre.

## 4.2 Distribution of dark matter and baryonic mass

In this section, we study how the relative fractions of stars, dark matter, and gas of a galaxy change as a function of its location around the halo in phase space. In particular, we look at the dark matter and gas mass ratios for the three different galaxy populations defined previously. Primarily, inside the halo, we expect there to be two effects of significance that affect the galaxy star formation property. The removal of gas due to ram-pressure, heating, etc. and the general tidal disruption of the extended dark matter halo leading to a reduction in dark matter mass.

First, in Fig. 6, we see how the dark matter mass ratio changes for the three different populations as we move closer to the centre of the host cluster halo. The curves in the figure show the ratio of the dark matter mass at a given radius to the median dark matter mass between 2 and $7 R_{200m}$. We note that while the massive Red galaxies and the Blue galaxies show a steady fall-off of dark matter mass ratio as we move towards the centre, as is expected from tidal disruption of haloes, the $Red_{low}$ galaxies appear to show an increase roughly near $\sim R_{200m}$, before the mean mass begins to drop. To investigate the origin of this effect, we look at the distribution of the mean total mass of galaxies at different locations in phase space. In the lower plot of Fig. 6, the $Red_{low}$ galaxies between pericentre and splashback appear to have higher total mass than elsewhere in the sample. A possible explanation for this effect is the quenching of Blue galaxies into low-mass Red galaxies between first pericentre and first apocentre (splashback); We divide our galaxies into populations based on their present-day colour and total masses, and Blue galaxies tend to have higher total mass than low-mass Red galaxies (see Fig. 1). Therefore,
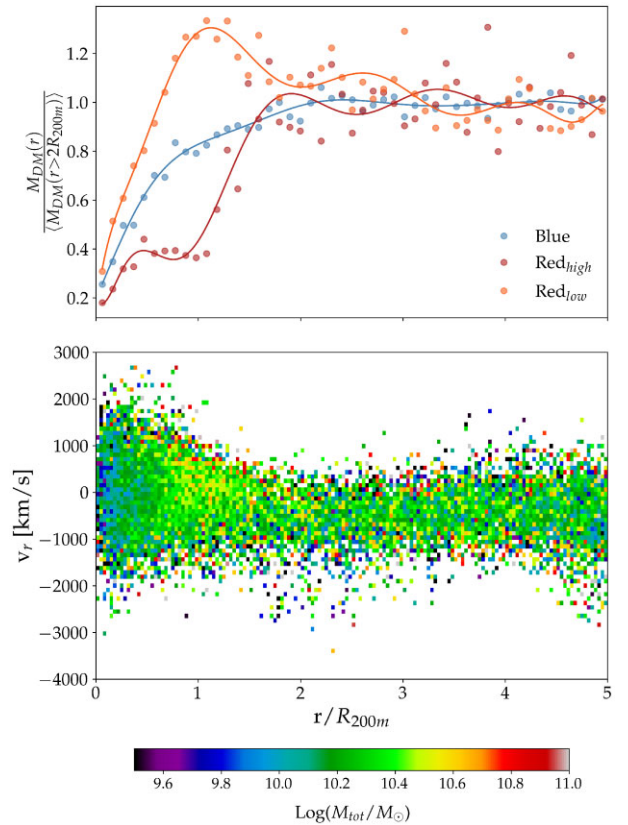


**Figure 6.** *Top*: The points indicate the ratio of the median dark matter mass of galaxies in radial bins to the median dark matter mass outside the cluster, between 2 and $7 R_{200m}$. The ratio is plotted for each of the three colour-mass populations at $z = 0.52$. The solid lines show a polynomial fit to the points. Blue and $Red_{high}$ galaxies have strictly decreasing dark matter masses as they fall into cluster centres. The $Red_{low}$ population displays a higher dark matter mass ratio between pericentre and splashback, before decreasing towards the centre. This is potentially due to the quenching of infalling Blues into Red. *Bottom*: $Red_{low}$ galaxies in phase space, weighted by the mean total mass of the galaxies in each bin. A triangular region of distinctly higher total mass is visible near $R_{200m}$, likely a result of the same effect causing the dark matter fraction to increase at the same radii.
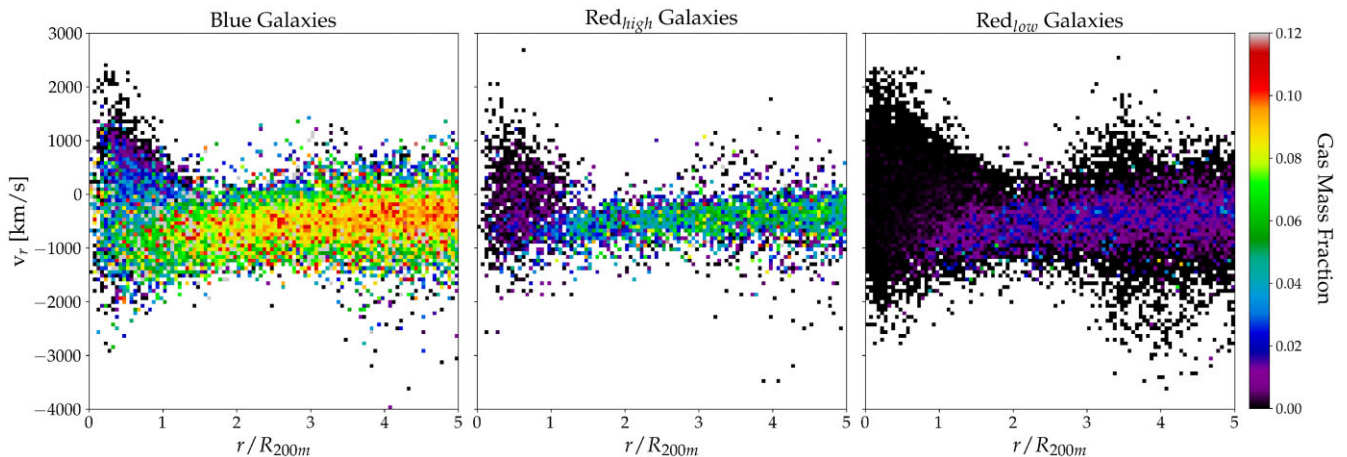
**Figure 7.** Stacked phase space diagrams for the three colour populations (Blue, Red$_{low}$, and Red$_{high}$ going from left to right) at $z = 0.52$, with each bin in the 2d histogram weighted by the mean ratio of gas mass to total mass of the galaxies in that bin. Blue galaxies have the highest proportions of gas, with higher velocity galaxies having less gas. The effects of gas stripping in cluster interiors are clearly visible as blue galaxies in the multistreaming region lose nearly all of their gas. Red$_{high}$ galaxies demonstrate a similar behaviour to the Blue galaxies. Red$_{low}$ galaxies also lose what little gas they have as they fall in. Note that Red$_{low}$ galaxies with the high radial velocities in the infall stream show a level of gas stripping comparable to those in the cluster interior, suggesting they were pre-processed as parts of smaller clusters.

a recently quenched galaxy, if on its first orbit with relatively low tidal disruption, might appear red but still have a significantly high total mass. We note that the radial distribution of the total mass, that can be probed by observations like weak lensing of satellite galaxies, carries information about the evolution of galaxy quenching.

In Fig. 7, we plot the mean gas mass fraction of galaxies at every location in phase space. The three different populations show significantly different behaviour that is reflective of their evolutionary history in the halo. The Blue galaxies, that are star forming, naturally tend to have the highest gas mass fractions among the different populations. In the infall stream these galaxies have nearly 10 per cent of their total mass made of gas. As we move within the halo, we note that post-pericentre the gas mass fractions appear diminished. This can be explained by the gas being severely stripped once the galaxies fall into the cluster host, due to effects like ram-pressure stripping, which should strongly depend on orbital history and leave a signature on the phase space. Similarly, we note that the Red$_{low}$ galaxies inside the cluster multistreaming region seem to have lost almost all of their gas. We also note that, although galaxies in the infall stream overall have higher gas mass fractions, the Red$_{low}$ galaxies that lie in the extended clouds tend to have gas mass fractions comparable to those that are within the clusters. This shows that a fraction of the galaxies that fall in as a part of groups have already lost significant amounts of their gaseous haloes. The Red$_{high}$ galaxies, which we expect to be centrals of groups, tend to have gas fractions significantly higher than Red$_{low}$ galaxies but lower than Blue galaxies in the infall stream. Red$_{high}$ galaxies show a general decrease of gas fraction within the cluster similar to the other two population. We note that the Red$_{high}$ in the multistreaming region seem to show lower gas fractions for galaxies in the positive velocity stream as they lose gas after pericentre passage. explanation. In Appendix B, we also show how other properties, such as the dark matter mass fraction and the black hole mass fractions, behave in phase space.

The various evolutionary histories of galaxy star formation leave distinct signatures on the phase space of dark matter haloes. As the radial number density profile of galaxies is simply an integration of the phase space along the radial velocity direction, these distinct pathways will leave specific signatures on the density profiles of

galaxies and their shapes. In the next section, we analyse how the various properties of galaxies affect the profile shapes and their slopes.

# 5 RADIAL DISTRIBUTION OF GALAXIES AND SPLASHBACK RADIUS

At a given redshift, we use the following procedure to produce a single galaxy number density profile for a given population of galaxies. For each halo, we compute the spherically averaged galaxy number density profiles in 15 logarithmically spaced radial bins. The bins extend to $7\,R_{200m}$ for each individual cluster, as opposed to a fixed physical distance as in other works. This allows for a higher signal-to-noise result when stacking the profiles, as the splashback radius scales with cluster properties like $R_{200m}$. The individual cluster profiles are stacked to produce a single average profile. The covariance matrix and error bars on the profiles are calculated using the Jackknife resampling method (Norberg et al. 2009).

## 5.1 Model fitting of galaxy number density profiles

We model the galaxy number density profiles using the fitting formula described in (Diemer & Kravtsov 2014). The 3d galaxy number density profile is defined by a virialized Einasto component and an outer infall component with some transition region (Einasto 1965). This is expressed as

$$\rho(r) = \rho_{inner}(r) f_{trans}(r) + \rho_{outer}(r). \qquad (2)$$

These terms are given by the following equations:

$$\rho_{inner} = \rho_s \exp\left(-\frac{2}{\alpha}\left(\left(\frac{r}{r_s}\right)^\alpha - 1\right)\right), \qquad (3)$$

$$f_{trans}(r) = \left[1 + \left(\frac{r}{r_t}\right)^\beta\right]^{-\gamma/\beta}, \qquad (4)$$

$$\rho_{outer}(r) = \rho_0 \left(\frac{r}{r_0}\right)^{-s_e}. \qquad (5)$$

**Table 2.** Prior ranges for the eight model parameters. $\mathcal{N}(x, \sigma^2)$ is a Gaussian prior with mean $x$ and standard deviation $\sigma$. We do not include a miscentring parameter.

| Parameter | Prior |
|---|---|
| $\log\left(\frac{\rho_s}{h^3\,\mathrm{Mpc}^{-3}}\right)$ | $[-8.0, 8.0]$ |
| $\log\left(\frac{\rho_0}{h^3\,\mathrm{Mpc}^{-3}}\right)$ | $[-8.0, 8.0]$ |
| $\log\left(r_s[h^{-1}\,\mathrm{Mpc}]\right)$ | $[\log(0.1), \log(5.0)]$ |
| $\log\left(r_t[h^{-1}\,\mathrm{Mpc}]\right)$ | $[\log(0.1), \log(5.0)]$ |
| $\log(\alpha)$ | $\mathcal{N}(\log(0.22), 0.6^2)$ |
| $\log(\beta)$ | $\mathcal{N}(\log(6.0), 0.2^2)$ |
| $\log(\gamma)$ | $\mathcal{N}(\log(4.0), 0.2^2)$ |
| $s_e$ | $[0.1, 10]$ |

This is the model that is also used in the measurement of splashback radius from projected galaxy number density profiles (More et al. 2016; Baxter et al. 2017; Chang et al. 2018; Shin et al. 2019; Adhikari et al. 2021). However, unlike the data model, we do not include a term for cluster miscentring. Our model therefore has a total of eight parameters from the halo model (Diemer & Kravtsov 2014). The parameters $r_0$ and $\rho_0$ are degenerate with one another, thus we fix $r_0 = 1.5$ Mpc $h^{-1}$. We fit the 3d galaxy number density profile with the eight-parameter model above using a Markov chain Monte Carlo method implemented in the EMCEE package, along with a jackknife estimate of the covariance matrix, adopting a Gaussian likelihood. The priors for each parameter are specified in Table 2. Since the uncertainty on the density profiles from the simulation is relatively small, we only show the best-fitting curves in the subsequent sections.

## 5.2 Colour population profiles

We evaluate the galaxy number density profile around the cluster sample for the three colour populations in the redshift range $1 > z > 0$. The profiles and their corresponding slopes for three selected redshifts ($z = 0, 0.52, 1.0$) are shown in Fig. 8. To reiterate, these are stacked profiles for haloes with mass greater than $5 \times 10^{13}\,\mathrm{M}_\odot\,h^{-1}$. In the top panels, the measured density profiles and the best-fitting models using the DK14 profile are shown. The bottom panels show the logarithmic slope of the fitted profiles.[3]

The essential thing to note is that, at any given redshift, the location of the minimum slope of the density profile is sensitive to the properties of the galaxies and encode evolutionary information. The three different samples in our study, we expect, arise from three distinct evolutionary histories. Our work demonstrates that these histories leave characteristic signatures in their radial distributions around the clusters.

*Red galaxies:* First, we note that the splashback radius of the $\mathrm{Red}_{\mathrm{low}}$ galaxies extends farthest out in units of $r/R_{200\mathrm{m}}$ at all redshifts. At $z = 0.52$, for example, the splashback radius of $\mathrm{Red}_{\mathrm{low}}$ galaxies is 25 per cent higher than the total profile. We expect these galaxies to trace the full extent of the dark matter multistreaming region of the phase space. Note that Fig. 5 shows that galaxies, after pericentric passage tend to get subsequently less blue with time, therefore the galaxies that do survive to the phase space boundary, or splashback radius, are preferentially red (as blue galaxies also transform to red).

---

[3]Note that the profiles decrease in amplitude with redshift. This is due to the fact that $\rho_g$ is calculated in bins defined by $R_{200\mathrm{m}}$ which increases at lower redshift.

Moreover, while the most radial orbits reach the farthest distances at splashback (Diemer 2017; Banerjee et al. 2020), they are also likely to be quenched faster than less radially orbiting galaxies, due to the smaller pericentres where they experience higher pressure drag.

The $\mathrm{Red}_{\mathrm{high}}$ population shows significantly different behaviour from their low-mass counterparts. The location of the minimum slope for this population is shifted to a smaller radii with respect to the full population. For $z = 0.52$, the splashback radius of $\mathrm{Red}_{\mathrm{high}}$ is 22 per cent lower than the All-galaxy profile. This can be understood as these massive galaxies are drawn towards the centre due to dynamical friction. The location of their minimum in slope in fact corresponds to the 'splashback' radius of that population, i.e. the apocentre itself is drawn to a smaller radius.

*Blue galaxies:* We find that the Blue galaxies show a shallower splashback feature as compared to either of the Red galaxy populations, however, we do not see similar results to blue galaxies from (Shin et al. 2021) or (Adhikari et al. 2021). For $z = 0.52$, the splashback radius of Blue galaxies is 30 per cent lower than that of the All-galaxy profile. Blue galaxies have a very shallow inner profile, that becomes shallower at later times: at $z = 0$, the slope becomes zero (flat density) deep inside the cluster. The location of the minimum slope is significantly lower than that of the $\mathrm{Red}_{\mathrm{low}}$ galaxy profile and the All-galaxy profile, but is relatively close to that of the $\mathrm{Red}_{\mathrm{high}}$ population. In Section 5.3, we discuss how the behaviour of the blue galaxies compares to data and discuss possible reasons for the shallower slope and prominent slope minimum of the Blue galaxy profile in IllustrisTNG.

We note that the relative trend in the location of the minimum slope between different galaxy colours holds as a function of redshift (Fig. 9). Overall, the comoving radius of the minimum slope falls as a function of redshift for all populations. However, in units of $r/R_{200\mathrm{m}}$, it remains fairly constant. In the bottom panel of Fig. 9, we plot the depth of the slope-minimum as a function of redshift. The splashback feature remains at a constant depth for the All-galaxy profile but gets shallower at late times for all of the colour-mass populations. This depth evolution is most extreme for the $\mathrm{Red}_{\mathrm{low}}$ population. The shallow nature of $\mathrm{Red}_{\mathrm{low}}$ splashback at late times is due to the higher density of $\mathrm{Red}_{\mathrm{low}}$ galaxies outside the splashback radius that are in smaller groups before infall into the massive clusters considered here. The depth of splashback radius is thus sensitive to the density of galaxies in the neighbourhood of the cluster.

*Summary:* Red galaxies in a cluster are not a uniform population, but originate from three different channels. The massive galaxies that are centrals of accreted group mass haloes have quenched mostly before infall and their splashback is shifted to a smaller radius compared to the total population. The low-mass Red galaxies are (i) either brought in by these groups, pre-processed previous to infall as can be seen in the large velocity clouds in the infall region of Fig. 4, or (ii) are the remnants of Blue galaxies that have quenched in the cluster themselves. The Blue and $\mathrm{Red}_{\mathrm{low}}$ galaxy outer slopes are therefore probes of quenching within clusters.

## 5.3 Comparison with data

In this section, we compare the galaxy number density profiles from IllustrisTNG with results from Shin et al. (2019) and Adhikari et al. (2021). Both these studies use the Sunyaev–Zeldovich (SZ)-selected clusters and DES galaxies to measure the cluster–galaxy correlation function. The mean mass of the sample in Adhikari et al. (2021) is $M_{200\mathrm{m}} = 3 \times 10^{14}\,h^{-1}\,\mathrm{M}_\odot$. Because there are very few clusters in the small volume of IllustrisTNG we select a halo sample of $M_{200\mathrm{m}} > 10^{14}\,h^{-1}\,\mathrm{M}_\odot$ to compare with data. We select only subhaloes
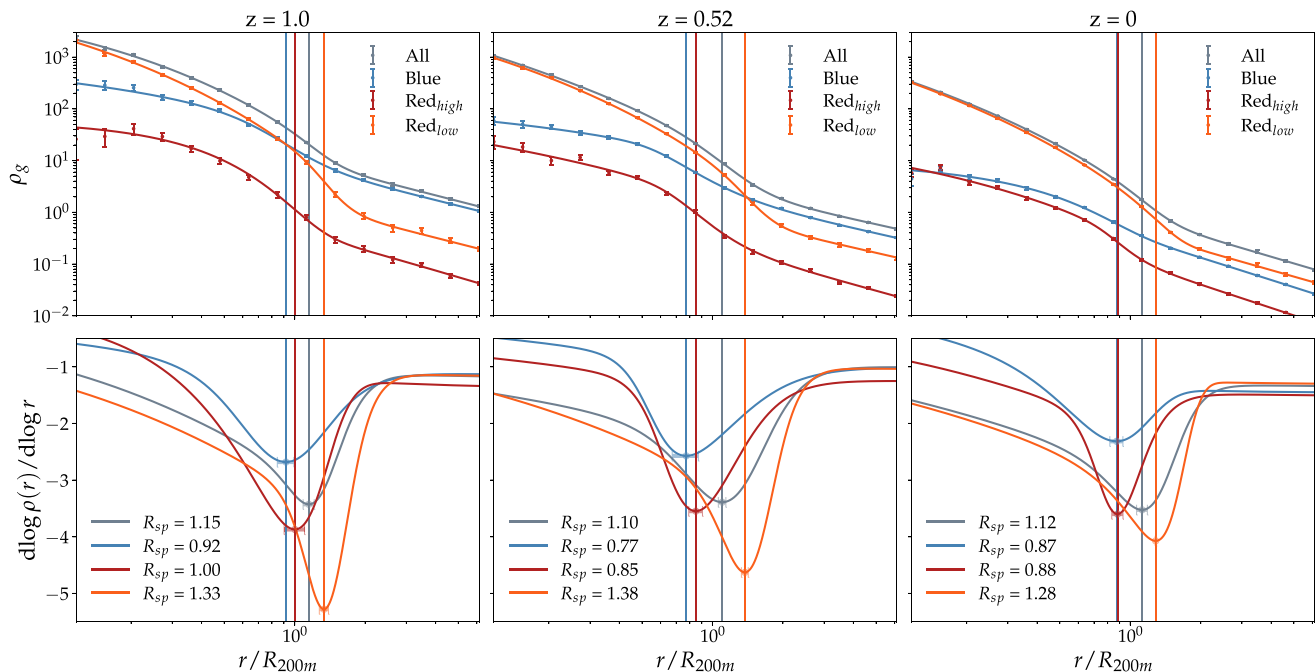
**Figure 8.** Galaxy number density profiles at $z = 1.0$, $0.52$, $0$ (left to right) for each of the three different colour-mass populations (upper panels), with their corresponding fitted logarithmic slope profiles (lower panels). The splashback radius, defined as the minimum of the slope, is shown by the vertical line. The profiles are given for each of the three colour split populations as well as the total profile, as indicated in the legend in the upper panels.

with an $i$-band magnitude brighter than $-19.87$ and non-zero total mass. We then attempt to select three similar colour populations by using only $g - r$ colour, instead of colour-space as in Adhikari et al. (2021). For this purpose, we define blue galaxies as those with $g - r < 0.4$, green as those with $0.4 < g - r < 0.55$, and red as those with $g - r > 0.55$. In the left-hand panel of Fig. 10, we overplot the Atacama Cosmology Telescope (ACT) results for galaxy splashback by colour from Adhikari et al. (2021) with results from similar colour cuts imposed on a similar sample from IllustrisTNG.

We find that the splashback radius of the red IllustrisTNG profile is similar to the red data splashback radius; however, the splashback signal in IllustrisTNG is significantly stronger, indicating a steeper fall off of the profile at the splashback radius. The shape of the log derivative is remarkably close, with the slopes in inner regions agreeing exceptionally well. Similarly, we note that the slope minimum for green galaxies agrees well with the data. However, we note that the green galaxies have a steeper profile than that observed in data within the halo.

For the blue profiles, we see significant differences between IllustrisTNG and observed clusters. Adhikari et al. (2021) and Shin et al. (2019) found no evidence of a feature at the splashback radius for blue galaxies, implying that blue galaxies do not survive to reach their first orbital apocentre – the measured density profile remains at least as steep as the infall profile well within the splashback radius. There is a shallow minimum, thought to be associated with their quenching and ceasing to be classified as blue galaxies. In IllustrisTNG, we see a deeper slope-minimum and a much shallower inner profile compared to observed clusters. A combination of rapid quenching along mostly radial orbits, combined with a significant population of blue galaxies with more tangential orbits, could provide a possible explanation for these differences. A rapid quenching process of blue galaxies on radial orbits (in particular, if a large fraction of galaxies within a radius at some fraction of $R_{sp}$ undergo severe environmental

quenching) would suppress their density, causing the slope of the number density profile in the inner regions to approach zero. Blue galaxies on non-radial orbits (such orbits have smaller apocentres than the most radial ones), would quench more slowly – presumably after reaching apocentre – and thus steepen the profile at radii slightly smaller than $R_{sp}$. Much of this discussion is supported by the phase space diagrams of Fig. 7 which show the fractional gas mass-loss of the three galaxy types. This suggests that the quenching of galaxies on radial orbits is more rapid in IllustrisTNG than in data, while those on more tangential orbits take a longer time to quench. We also note that the effect of projection in going from 2d to 3d may play a role in comparing with observations.

In order to further probe the differences between blue galaxies in IllustrisTNG and data, we follow the analysis of Shin et al. (2019) by determining the splashback of two populations that result from the splitting of the blue population into evenly split lower and higher $g - r$ groups (Shin et al. 2019). We do this as a further check of how colour quenching is related to splashback and the time a galaxy has been inside the cluster. The right-hand panel of Fig. 10 shows the results of a comparison to South Pole Telescope (SPT) data. The SPT data uses a host halo sample with $\langle M_{500c} \rangle = 3 \times 10^{14} \, h^{-1} \, \mathrm{M_\odot}$. In this comparison, we revert to our fiducial host halo mass cut of $5 \times 10^{13} \, h^{-1} \, \mathrm{M_\odot}$ in order to obtain good statistics in the simulation volume. As in Shin et al. (2019), we find that the 'most blue' galaxies display a shallower slope minimum, at a smaller radius than the 'less blue' galaxies. However, the difference between the depth and location of the slope minima in IllustrisTNG is much less significant. Both blue populations in IllustrisTNG have more distinct slope minima and significantly shallower inner regions than in SPT data. Since no subset of the blue galaxies mirrors the slope of the profiles in data, we emphasize the argument that there are inherent differences between the blue galaxy population in IllustrisTNG and in data.
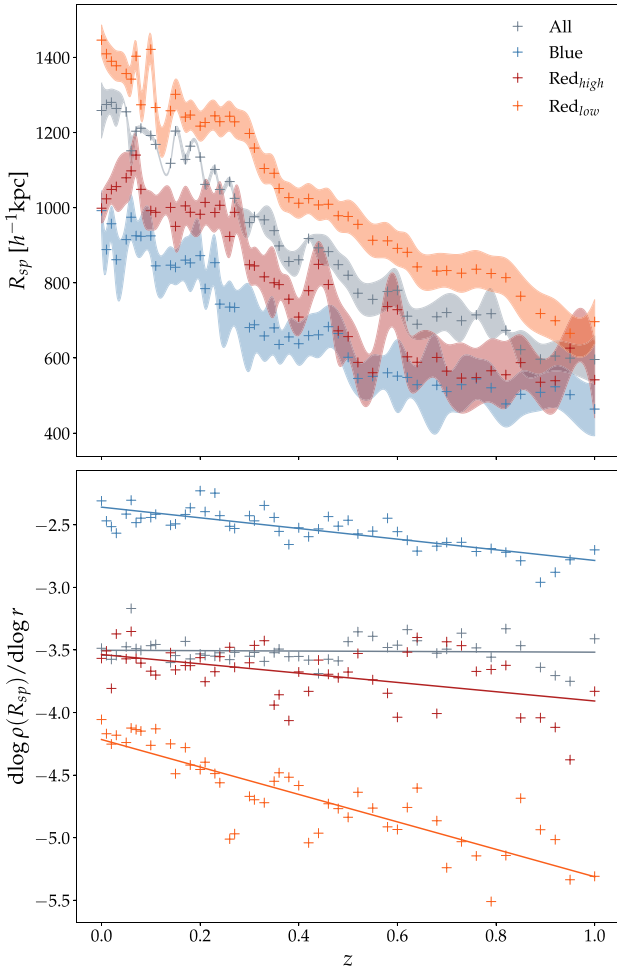
**Figure 9.** Evolution of the splashback radius over redshift. The upper panel displays the evolving value for $R_{sp}$ in comoving units (kpc $h^{-1}$) for the three colour-mass populations and all galaxies in our sample between $z = 0$ and $z = 1$. The uncertainty in $R_{sp}$ is represented as the shaded region around the lines for each population. The lower plot displays the evolution of the minimum of the logarithmic slope of the galaxy number density profile. Linear fits are included as solid lines. Note that at all times the Red$_{low}$ population has the largest splashback radius.

We note also that the slope profile for the full galaxy sample (grey solid line in the left-hand panel of Fig. 10) agrees statistically with data (grey shaded) near the splashback region. This was also shown in Shin et al. (2021). Both in the outer and inner regions there are however significant differences. In particular in the outer region the slope is significantly shallower in IllustrisTNG compared to data. As the slope in the outer region can be thought to be set essentially by free fall on to a massive cluster (Baxter et al. 2017), this difference could possibly arise due to differences in the overall shapes of the two samples (Lithwick & Dalal 2011). More massive clusters (like those in data) are more elliptical than their lower mass counterparts and ellipticity can significantly affect the outer slopes in the direction seen here (Lithwick & Dalal 2011). Projection effects in data may also play a role. We defer a thorough investigation of this effect to future work. The differences in the inner region may be related to differences in galaxy disruption between the simulation and data.

## 5.4 Splashback and galaxy luminosity: effects of dynamical friction and self-friction

In this section, we briefly explore the effects of changing the absolute magnitude selection of the galaxy sample on the splashback feature. As discussed above, one of the potential explanations for the shift to lower splashback radii in high-mass Red$_{high}$ galaxies in our fiducial host cluster sample is dynamical friction. Dynamical friction, through an effective drag force, can slow massive galaxies down and cause second turnaround to occur at a smaller radius. In particular, dynamical friction is known to bias the splashback radius w.r.t particles when the galaxies live in subhaloes with total mass greater than 0.01 times the host mass (Adhikari, Dalal & Clampitt 2016; More et al. 2016).

First, we split our galaxy sample into three cumulative total mass bins and fit number density profiles in the left-hand panel of Fig. 11. For this analysis, we revert back to our fiducial sample of clusters with $M_{200m} > 5 \times 10^{13}\,h^{-1}\,M_\odot$. The two lower mass bins do not demonstrate a shift in slope minimum but the highest mass bin with $M_{tot} > 10^{11}$ displays a visible shift towards a lower splashback radius. These galaxies live in subhaloes that are around 0.01 the mean host mass, and a shift is therefore expected. Note that the total mass in IllustrisTNG is the current subhalo mass, which has presumably lost a fraction of its mass since infall. Therefore, its pre-infall mass is expected to be even higher.

To compare with observational work in Chang et al. (2018), we conduct a similar analysis but split the galaxy sample using absolute magnitude in the $i$ band in the middle panel of Fig. 11. Chang et al. (2018) did not find significant evidence for movement of the splashback radius with galaxy magnitude, even though abundance matching of their galaxy sample to CDM-only simulations implied that such a movement should be seen.

Curiously, even though the RedMaPPer (Rykoff et al. 2014) optically selected cluster sample in Chang et al. (2018) is expected to suffer from systematics, we see a similar trend in IllustrisTNG. Our magnitude binned samples show virtually no difference in splashback radii with $i < -19.4$ and $i < -20.4$ bins displaying almost identical splashback features while our highest magnitude bin, $i < -21.4$ has a significantly deeper splashback. We include one sample with $i < -16$ which can be considered as almost all subhaloes (and therefore dominated by the lower mass ones), which has a higher splashback radius than the other three bins and is expected to be comparable to the splashback in particles as seen in fig. 6 of Shin et al. (2021). We note that the splashback in total mass and that of the faintest galaxy sample is shifted to a larger distance with respect to the brighter galaxies.

In the rightmost panel of Fig. 11, we plot the peak mass distribution of the galaxies in the different magnitude bins. We select a sample of 1000 galaxies from our subhalo sample randomly from within each magnitude for a total of 4000 galaxies, then using the LHaloTree, we track their total mass through time and evaluate their peak masses before infall. The black dashed line is at $0.01M_{host, min}$ or $5 \times 10^{11}$ $h^{-1}\,M_\odot$. As is observed, there is significant scatter in the peak total mass in each sample with a magnitude threshold. Therefore, it is possible that all galaxies with magnitudes greater than $M_i < -19$ show effects of dynamical friction. Only a small fraction of the $M_i < -16$ samples has masses above $0.01M_{host, min}$. While dynamical friction may explain the shift between the overall particle splashback and galaxies, it is still unclear why the galaxy splashback remains static between the different brighter galaxy samples.

It is important to emphasize another possible cause for the shift to smaller splashback radii: the effect of dynamical self-friction.
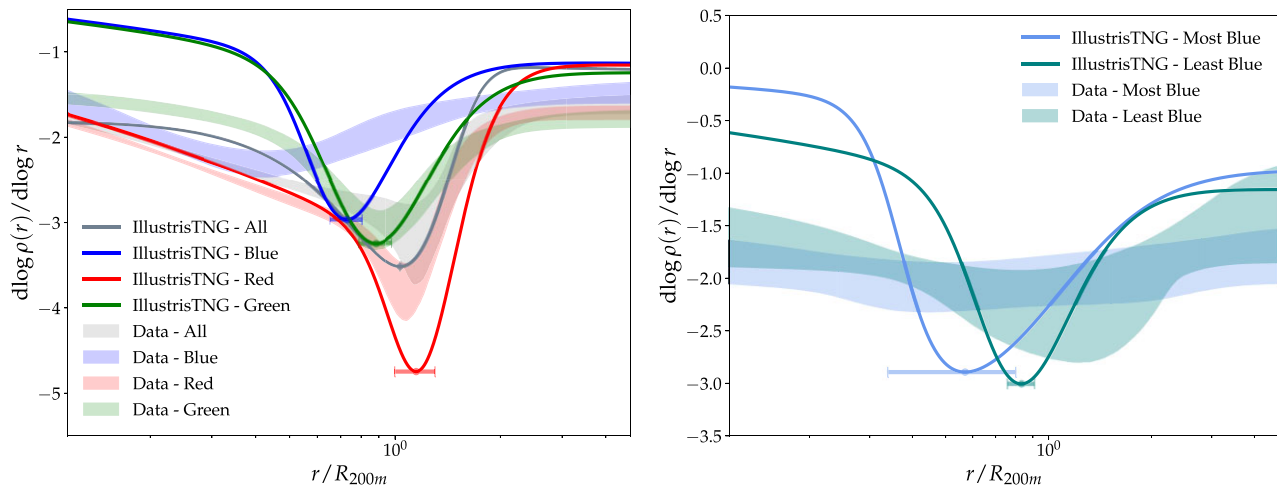
**Figure 10.** *Left*: Fitted slope of the 3d galaxy number density profiles split by colour, comparing observational data from Adhikari et al. (2021) to similar colour and magnitude cuts in IllustrisTNG. The shaded curves are measurements from data, and the solid curves are from IllustrisTNG. The location of the minimum slope of red and green galaxies in IllustrisTNG agree well with the data, while the blue galaxy population minimum slope looks different. We discuss further comparisons in Section 5.3. *Right*: Fitted slope for 3d galaxy number density profiles of Blue galaxies split into bluer and less blue sub-populations, comparing observational data to similar cuts made in IllustrisTNG. IllustrisTNG exhibits steeper and more distinct slope minima at smaller radii than data, particularly for the most blue population. The inner regions are also significantly shallower in IllustrisTNG. (Note that the cluster mass threshold in IllustrisTNG is slightly lower than the threshold in data. This is in order to obtain good statistics in the simulation volume.)
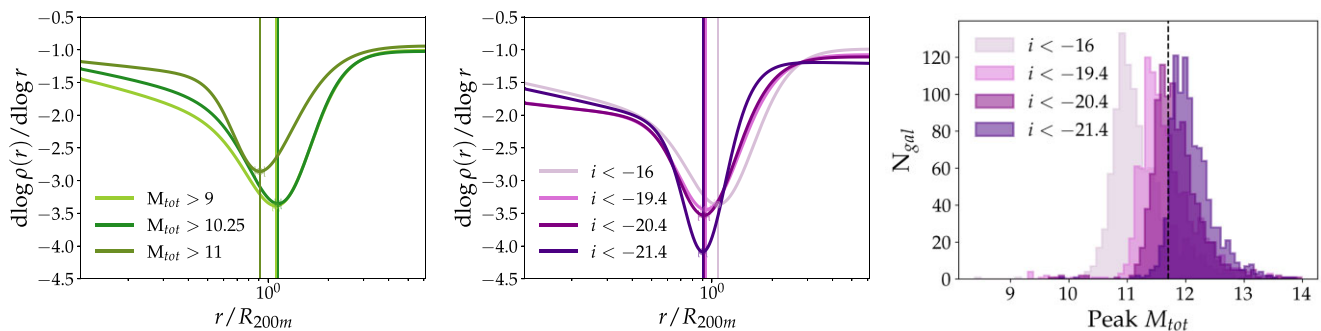


**Figure 11.** *Left*: Fitted slope of 3d number density profiles as a function of total mass (all galaxies split into three mass bins: greater than $10^9$, $10^{10.25}$, $10^{11} \, h^{-1} \, \mathrm{M_\odot}$). The lower splashback radius of the highest mass bin is consistent with the effects of dynamical friction. *Middle*: Fitted slopes of all galaxies in our sample split into four bins based on $i$-band magnitude ($i < -16$, $i < -19.4$, $i < -20.4$, $i < -21.4$). The $i < -16$ profile can be considered similar to the All-galaxy profile in our usual sample. The other three magnitude bins have very similar values for splashback. Thus, splitting galaxies by their absolute magnitude does not seem show effects of dynamical friction. *Right*: Peak $M_{tot}$ distributions for the same $i$-band splits used in the middle plot. The black dashed line indicates $M_{tot} = 0.01 M_{host,min}$ where $M_{host,min} = 5 \times 10^{13} \, h^{-1} \, \mathrm{M_\odot}$ is the minimum total host mass. See the text for further discussion.

Dynamical self-friction is an effect that can cause a significant reduction in the orbital angular momenta of subhaloes due to the torque exerted by material stripped from themselves. It can potentially dominate over dynamical friction along more radial orbits and close to pericentric passage (Miller et al. 2020). Work done by Miller et al. (2020) found that in simulations, massive subhaloes in particular experience this self-friction. It causes subhaloes to spiral towards the centres of host clusters, an effect which, like dynamical friction, could potentially reduce the apparent splashback radius of an affected galaxy population. A quantitative study of the interactions of dynamical friction and self-friction as a function of halo mass, splashback, and infalling groups in IllustrisTNG would be able to shed more light on the relative impact of this effect.

Note that O'Neil et al. (2021) also found that the splashback radius was around 12 per cent lower in galaxy number density profiles as compared to dark matter profiles for a cluster sample between $10^{13}$ and $10^{13.5} M_\odot$. They attributed this difference to dynamical friction.

We see a difference of similar degree in our absolute magnitude split samples between the $i < -16$ and the higher magnitude bins, implying that friction effects must be taken into account when dealing with cluster samples that are closer to group sized haloes.

## 6 CONCLUSION

We have studied the evolution of galaxies in galaxy clusters in the IllustrisTNG 300-1 simulation and connected them to observable signatures in their number density profiles, phase space distributions, and splashback radius. Our study has two additional goals: (1) to understand IllustrisTNG's galaxy populations using these observables and to compare them with observations from DES, and (2) to use the phase space, colour, and luminosity distributions of galaxies to test our methodology of connecting quenching during galaxy infall into clusters with their radial profiles [see Adhikari et al. (2021)].

Hydrodynamical simulations offer a useful test of the methodology since quenching is implemented in a physical way in contrast to N-body simulations. Finally, we also explore the effect of dynamical processes like dynamical friction and self-friction on the distribution of galaxies.

We use Gaussian mixture models in the space of colour and total mass to identify three distinct galaxy populations: Blue, $Red_{low}$ and $Red_{high}$. We compare these with the populations studied in previous work. We explore how the different evolutionary channels for the three types of galaxies leave signatures on the overall colour distribution of the galaxies in the universe and in the environment of galaxy clusters. We also make preliminary comparisons with existing data on galaxies observed with the DES optical survey around massive clusters identified via their SZ signal in the ACT and SPT surveys. We find that, on average, $Red_{high}$ galaxies originate as Blue galaxies that increase significantly in mass and then undergo a fast quenching process at a certain mass threshold, consistent with 'mass quenching' which typically occurs due to AGN feedback while these galaxies infall as centrals of groups. $Red_{low}$ galaxies originate as Blue galaxies that redden with time in the dense environments of either infalling groups or the clusters. These two different paths reflect the mass and environmental quenching experienced by high- and low-mass Red galaxies, respectively. We study in detail how these galaxies occupy the phase space of cluster haloes.

We also study their impact on the density profile of clusters, which is observed in projection in multicolour imaging surveys. Massive Red galaxies, ($Red_{high}$), falling in as centres of groups with large subhalo masses, tend to sink to the centre of the cluster due to the combined effects of dynamical friction and self-friction. These galaxies therefore appear to have a significantly smaller splashback radius compared to the full galaxy population. In addition, $Red_{high}$ galaxies, which are predominantly already red *before* infall, lose all of their gas mass within the virialized region of the cluster.

The Blue galaxies in the vicinity of a cluster primarily live in the infall stream. They show a clear loss of gas fraction as they traverse the phase space within the cluster halo (see Fig. 7). In IllustrisTNG, there are very few Blue galaxies with radial orbits that cross pericentre and remain star forming – we find that the highest positive radial velocity envelope in phase space is missing Blue galaxies which have converted into low-mass Red galaxies. Their phase space boundary, between multistreaming and infall, is therefore also at a smaller radius than the splashback boundary of the halo. Therefore, the farthest boundary of the halo is made of $Red_{low}$ galaxies. Thus, low-mass $Red_{low}$ galaxies sample the complete phase space of dark matter in a halo (barring disruption of a small fraction in the innermost region). In other words, all possible phase space locations of dark matter should be most closely sampled by the low-mass $Red_{low}$ galaxies. A significant fraction of the $Red_{low}$ galaxies are also brought in as part of groups, this fraction increases at late times.

While the above discussion focused on the different colour populations, we emphasize that the total galaxy profile closely traces that of the dark matter (when the galaxy magnitude threshold is not significantly affected by dynamical friction). The quenching induced changes in galaxy colour do not affect the shape of the total profile, keeping the total number of galaxies conserved. We note that the agreement of the total galaxy profile with the matter profile in Shin et al. (2021) is consistent with the idea that processes such as tidal disruption do not destroy a significant fraction of the galaxies in the sample. This finding has two direct implications: that if galaxies follow dark matter closely, they can be used to study halo properties, and deviations from the dark matter distributions of galaxy sub-populations help us study evolutionary processes.

Comparing DES galaxies around ACT and SPT clusters to the simulations revealed subtle differences between the galaxy populations (see Fig. 10). In particular, while the red and green galaxy splashback and radial profiles agree fairly well, the blue galaxies behave significantly differently from simulations. We find that the observational data prefers a scenario where the blue galaxy profile remains close to a power law from the infall regime down to the inner halo, with a shallow minimum inside the halo, implying that some blue galaxies cross pericentre and quench before apocentre. However in IllustrisTNG the profile flattens: the shallow slope in the inner regions shows that blue galaxies are either getting disrupted or completely quenched by pericentre. In addition, the sharper feature in the outskirts in IllustrisTNG is formed by a significant fraction of galaxies that are on higher angular momentum orbits. Therefore, it appears that for the simulation clusters, the quenching time-scale is shorter than that in observational data.

Our work suggests that the evolutionary histories of galaxies through their orbits around a halo leave distinct signatures on their phase space distribution. Observationally these signatures are encoded in the shape of radial number density profiles and also the projected velocity distributions. In particular, we note that the distribution of blue galaxies may be most informative about the quenching time-scales which likely depend both on the orbits and infall times. In future work we hope to constrain the orbit and infall time distribution of galaxies of different population using the rich data that is available. We note that in spectroscopic surveys we can jointly model the velocity and spatial distributions to constrain models of quenching and disruption. The local slope of the number density distribution alone also encodes much of the phase space information, making it a powerful probe of galaxy evolution in photometric surveys. Current surveys can measure these distribution out to $z = 1$ with high precision. Comparison to the dark matter distribution (Shin et al. 2021), or the gas distribution (Zinger et al. 2016; Anbajagane et al. 2021; Baxter et al. 2021) can help us distinguish between different intracluster processes that are relevant for galaxy evolution, help constrain models in hydrodynamic simulations, and fine tune our understanding of the galaxy–halo connection in clusters.

## ACKNOWLEDGEMENTS

## DATA AVAILABILITY

The data underlying this article will be shared on reasonable request to the corresponding author.

## REFERENCES

Abadi M. G., Moore B., Bower R. G., 1999, MNRAS, 308, 947

Adhikari S., Dalal N., Chamberlain R. T., 2014, J. Cosmol. Astropart. Phys., 1411, 019

Adhikari S., Dalal N., Clampitt J., 2016, J. Cosmol. Astropart. Phys., 1607, 022

Adhikari S., Dalal N., More S., Wetzel A., 2019, ApJ, 878, 9

Adhikari S. et al., 2021, ApJ, 923, 37

Aihara H. et al., 2018, PASJ, 70, S4

Anbajagane D. et al., 2021, preprint (arXiv:2111.04778)

Anbajagane D. et al., 2022, MNRAS, 510, 2980

Balogh M., Morris S. L., Yee H. K. C., Carlberg R. G., Ellingson E., 1997, ApJ, 488, L75

Banerjee A., Adhikari S., Dalal N., More S., Kravtsov A., 2020, J. Cosmol. Astropart. Phys., 02, 024

Baxter E. et al., 2017, ApJ, 841, 18

Baxter E. J., Adhikari S., Vega-Ferrero J., Cui W., Chang C., Jain B., Knebe A., 2021, MNRAS, 508, 1777

Chang C. et al., 2018, ApJ, 864, 83

Contini E., Gu Q., Ge X., Rhee J., Yi S. K., Kang X., 2020, ApJ, 889, 156

Davis M., Efstathiou G., Frenk C. S., White S. D. M., 1985, ApJ, 292, 371

Diemer B., 2017, ApJS, 231, 5

Diemer B., Kravtsov A. V., 2014, ApJ, 789, 1

Dolag K., Borgani S., Murante G., Springel V., 2009, MNRAS, 399, 497

Donnari M. et al., 2019, MNRAS, 485, 4817

Donnari M. et al., 2021, MNRAS, 500, 4004

Dressler A., 1980, ApJ, 236, 351

Dressler A., Gunn J. E., 1983, ApJ, 270, 7

Einasto J., 1965, Trudy Astrofiz. Inst. Alma-Ata, 5, 87

Fillmore J. A., Goldreich P., 1984, ApJ, 281, 1

Gunn J. E., Gott III J. R., 1972, ApJ, 176, 1

Larson R. B., Tinsley B. M., Caldwell C. N., 1980, ApJ, 237, 692

Lithwick Y., Dalal N., 2011, ApJ, 734, 100

Marinacci F. et al., 2018, MNRAS, 480, 5113

Miller T. B., van den Bosch F. C., Green S. B., Ogiya G., 2020, MNRAS, 495, 4496

More S., Diemer B., Kravtsov A., 2015, ApJ, 810, 36

More S. et al., 2016, ApJ, 825, 39

Murata R., Sunayama T., Oguri M., More S., Nishizawa A. J., Nishimichi T., Osato K., 2020, PASJ, 72, 64

Naiman J. P. et al., 2018, MNRAS, 477, 1206

Nelson D. et al., 2018, MNRAS, 475, 624

Nelson D. et al., 2021, preprint (arXiv:1812.05609)

Niemiec A., Jullo E., Giocoli C., Limousin M., Jauzac M., 2019, MNRAS, 487, 653

Norberg P., Baugh C. M., Gaztañaga E., Croton D. J., 2009, MNRAS, 396, 19

Oemler A., Jr, 1974, ApJ, 194, 1

Oman K. A., Hudson M. J., 2016, MNRAS, 463, 3083

O'Neil S., Barnes D. J., Vogelsberger M., Diemer B., 2021, MNRAS, 504, 4649

Pillepich A. et al., 2018, MNRAS, 475, 648

Planck Collaboration VI, 2018, preprint (arXiv:1807.06209)

Poggianti B., Smail I., Dressler A., Couch W., Barger A., Butcher H., Ellis R., Oemler A., Jr, 1999, ApJ, 518, 576

Popesso P. et al., 2018, MNRAS, 483, 3213

Rykoff E. S. et al., 2014, ApJ, 785, 104

Shi X., 2016, MNRAS, 459, 3711

Shin T. et al., 2019, MNRAS, 487, 2900

Shin T. et al., 2021, MNRAS, 507, 5758

Springel V., 2010, MNRAS, 401, 791

Springel V., White S. D. M., Tormen G., Kauffmann G., 2001, MNRAS, 328, 726

Springel V. et al., 2018, MNRAS, 475, 676

Terrazas B. A. et al., 2020, MNRAS, 493, 1888

The Dark Energy Survey Collaboration, 2005, preprint (arXiv:astro-ph/0510346)

Villaescusa-Navarro F. et al., 2016, MNRAS, 456, 3553

Weinberger R. et al., 2018, MNRAS, 479, 4056

Weinberger R., Springel V., Pakmor R., 2020, ApJS, 248, 32

Zinger E., Dekel A., Kravtsov A. V., Nagai D., 2016, preprint (arXiv:1610.02644)

Zürcher D., More S., 2019, ApJ, 874, 184

## APPENDIX A: HYDROGEN ABUNDANCE

We briefly examine the distributions of the three colour–mass populations in hydrogen abundance to further probe their diverging properties. Fig. A1 shows the hydrogen abundance of galaxies at $z = 0.52$ versus mass, weighted by the $g - r$ colour of the galaxy. Blue galaxies display a complicated relationship between hydrogen abundance, mass, and colour. Generally, the higher the mass, the lower the hydrogen abundance. The *bluer* (lower $g - r$) Blue galaxies are located at the extremes of the hydrogen to mass relationship. The most blue galaxies either have much higher proportions of hydrogen relative to mass compared to the average blue galaxy, or a much lower ratio. For example, along a line of constant mass at $10^{11} \, h^{-1} \, M_\odot$, the highest and lowest ends are occupied by the most blue galaxies. Meanwhile, redder Blue galaxies tend towards the median, rather than occupying one or the other extreme. This relation further suggests that galaxies which are initially blue quench into two
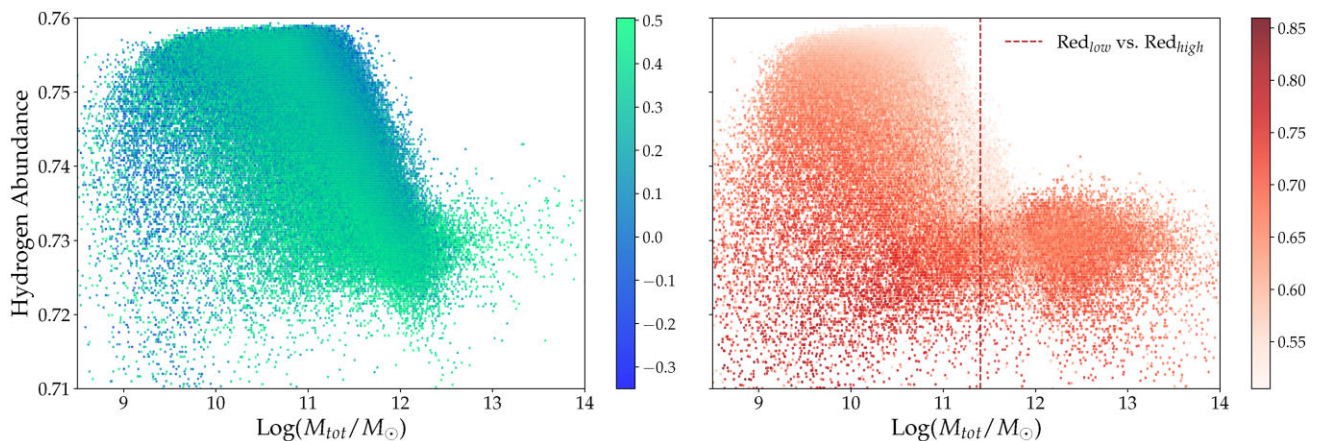


**Figure A1.** Hydrogen abundance of galaxies versus total mass, weighted by $g - r$ colour. The left plot considers Blue galaxies only, while the right plot shows all Red galaxies. The dashed red line in the right plot indicates the $z = 0.52$ cut defined in total mass between Red$_{low}$ and Red$_{high}$ galaxies. The bluer Blue galaxies are bifurcated between a low mass, lower hydrogen abundance region, and a higher mass, higher abundance region, in between which are redder Blue galaxies. In the right-hand panel, the vertical line indicating the split between Red$_{high}$, Red$_{low}$ also splits two distinct populations in abundance versus mass, such that Red$_{high}$ galaxies have a lower hydrogen abundance than the Red$_{low}$ population.

different populations based on their initial conditions, which can be visibly distinguished in Fig. A1. However, further work is necessary to determine how Blue galaxies in IllustrisTNG actually evolve in this hydrogen abundance – mass space.

The split in total mass between $Red_{low}$ and $Red_{high}$ is noted in the plot as the dashed red line. This split clearly separates Red galaxies with distinct behaviour in hydrogen abundance – mass space. $Red_{low}$ galaxies display a similar relationship between hydrogen abundance and mass as Blue galaxies, the higher the mass, the lower the hydrogen abundance. This correspondence between the properties of Blue and $Red_{low}$ galaxies reflects their behaviour on the SFMS. $Red_{high}$ galaxies, on the other hand, are clustered at a small range of low hydrogen abundances with little to no relationship between mass and abundance. This behaviour could align with the idea of $Red_{high}$ as the products of an internal mass-quenching process linked to AGN feedback as that feedback process has been linked to a reduction of the neutral hydrogen content of haloes in hydrodynamical simulations (Villaescusa-Navarro et al. 2016).

# APPENDIX B: DISTRIBUTION OF DARK MATTER AND BLACK HOLE MASS IN PHASE SPACE

We extend the discussion from Section 4.2 by examining the black hole and dark matter ratio distributions in phase space for the three colour-mass populations defined in Section 3.1. In Fig. B1, we show the stacked phase space with each bin weighted by the mean dark matter mass ratio (DM/total) for Blue, $Red_{high}$, and $Red_{low}$ galaxies. All three populations exhibit a trend of decreasing dark matter ratio towards the cluster centre, demonstrating dark matter stripping. Previous studies in the Illustris simulation have shown that dark matter stripping begins at around $1.5\,R_{vir}$ (Niemiec et al. 2019), which is also where we see the infall stream of phase space transition into the multistreaming region. However, we overall find a slightly more complicated picture for dark matter stripping, as $Red_{low}$ galaxies and Blue galaxies at high radial velocities and in the multistreaming region show higher dark matter mass fractions than galaxies in the infall stream. The initial peak in the $Red_{low}$ curve in
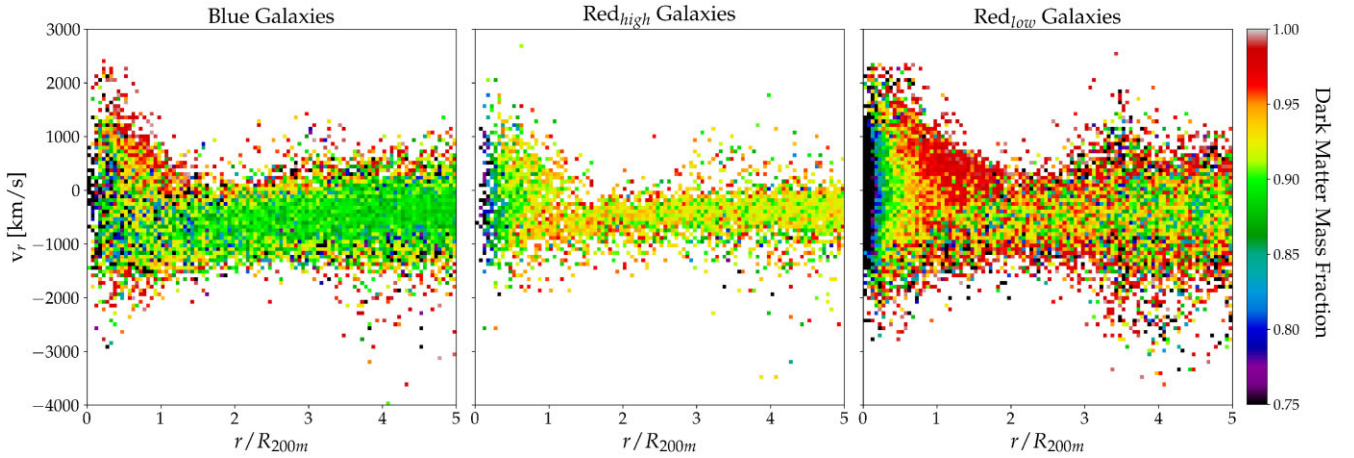


**Figure B1.** Stacked phase space for three colour-mass populations, where each panel is coloured by the mean ratio of mass of dark matter to total mass of the galaxies in a given bin. Note that the density of galaxies in each histogram bin is not represented in this plot. Blue galaxies have relatively constant ratios of dark matter, with higher ratios at higher velocities. $Red_{high}$ galaxies have decreasing ratios of dark matter to total matter as they enter the multistreaming region and fall into the cluster. $Red_{low}$ galaxies have varied amounts of dark matter in the infall stream, however have a higher dark matter ratio between pericentre and splashback than in infall, before rapidly decreasing in cluster interiors.
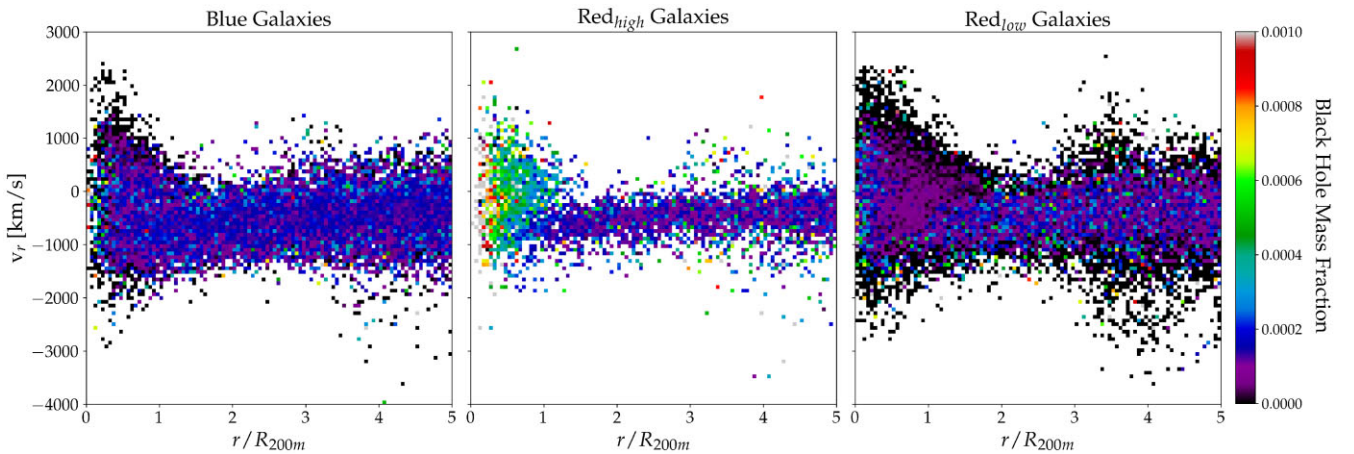


**Figure B2.** Stacked phase space for three colour-mass populations, where each panel is coloured by the mean ratio of black hole mass to total mass of the galaxies in a given bin. Note that the density of galaxies in each histogram bin is not represented in this plot. Blue galaxies and $Red_{low}$ galaxies have similar black hole ratios, with higher velocity galaxies have little to no mass contribution from black holes. $Red_{high}$ galaxies have higher black hole mass ratios towards cluster interiors.

Fig. 6 has a corresponding region visible as a red (high dark matter ratio) triangular area in the Red$_{low}$ DM fraction plot of Fig. B1, likely created by quenching of blue galaxies. The distinct higher dark matter ratio group of blue galaxies at higher radii reinforces the arguments made in Section 5.3 that there are significant differences in the quenching pathways of blue galaxies on radial and tangential orbits, which in turn impact the galaxy number density profiles. In Fig. B2, we similarly weigh each bin in phase by the black hole mass fraction for each of the three populations. We find further evidence for the distinct properties and quenching pathways taken by the two Red populations in their black hole mass fractions. Red$_{high}$ and Blue galaxies both display higher black hole mass fractions than Red$_{low}$ galaxies. This distinction between Red$_{high}$ and Red$_{low}$ galaxies supports the notion that Red$_{high}$ galaxies are products of mass quenching by AGN feedback rather than environmental quenching. The higher radial velocity sections of the Red$_{low}$ phase space have no black hole mass, further suggesting that they are undergoing infall as parts of smaller clusters.

## APPENDIX C: LINE-OF-SIGHT VELOCITY DISTRIBUTIONS

We study the LOS velocity distribution of the three populations as a function of radius from the cluster centre. The LOS velocity dispersion is also be a promising probe of galaxy evolution, particularly in spectroscopic surveys. They are also often used for mass calibration of clusters. We assume a flat sky approximation and use the $z$ component of the velocity of the galaxy w.r.t. to the cluster centre as the LOS direction such that,

$$\Delta v_{\mathrm{los}} = \frac{v_{\mathrm{gal}} - v_{\mathrm{cluster}}}{1 + z_{\mathrm{c}}}. \tag{C1}$$

We measure the LOS distributions for clusters at $z = 0.52$, in three bins of projected radii shown in Fig. C1. The three bins were chosen to represent the innermost regions of the cluster, near the splashback radius and in the infall region. In the infall regime (rightmost panel), Red$_{low}$ galaxies have strong tails, and the highest LOS velocity dispersion, this is because a significant fraction of them they fall in as parts of groups. Blue galaxies are primarily tracing the host clusters potential. In the innermost regions of the cluster, the blue galaxies and to some extent the Red$_{high}$ galaxies show an LOS distribution that appears to be composed of two distinct components, with a small and large dispersion. The low dispersion component peaked at $\Delta v_{\mathrm{los}} = 0$, is from galaxies on tangential orbits that have low LOS velocities at small projected radius. As discussed in the sections above, IllustrisTNG quenches radial blue galaxies, therefore a large fraction of galaxies that are blue will show this two-component LOS distribution.
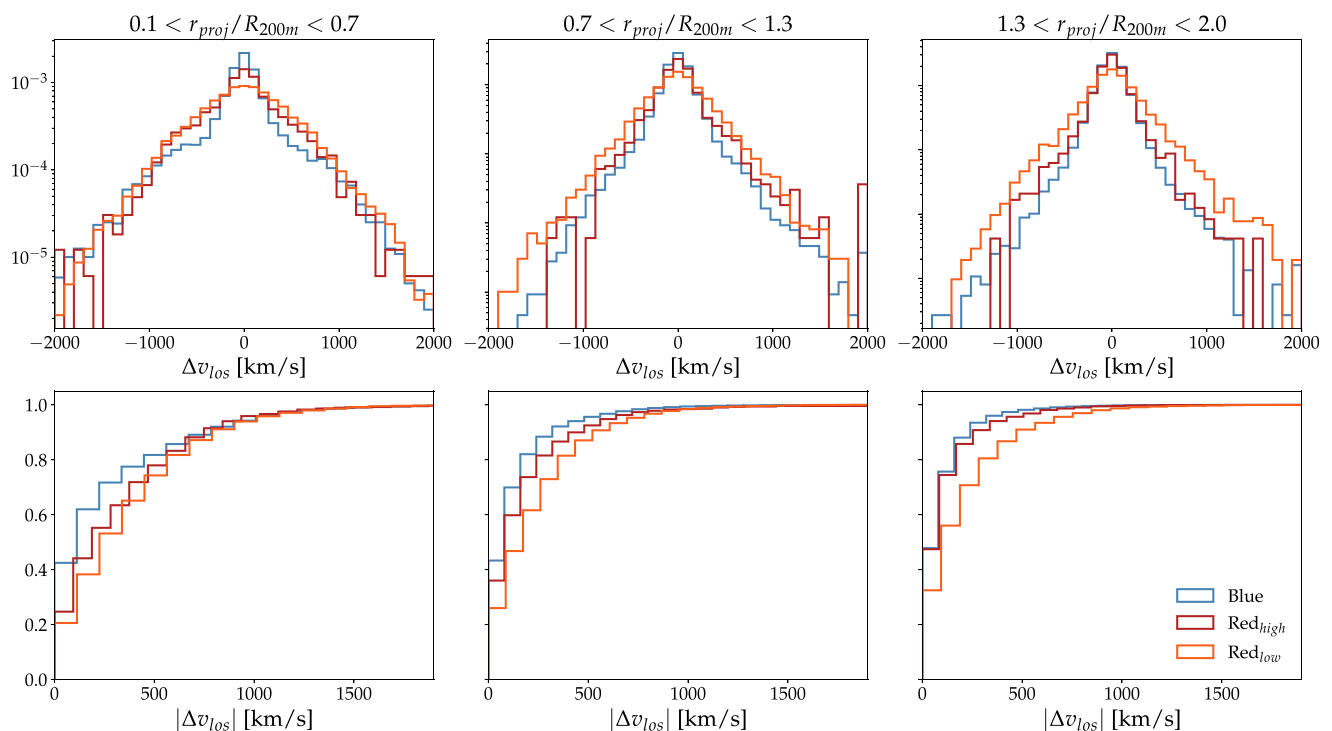


**Figure C1.** The LOS velocity distribution as a function of galaxy colour in three projected radial bins. The top panel shows the PDF and the bottom panel shows the CDF. The LOS distribution encodes signatures of galaxy evolution as discussed in the text.

This paper has been typeset from a T$_{\mathrm{E}}$X/L$^{\mathrm{A}}$T$_{\mathrm{E}}$X file prepared by the author.